



# Aurora in the Polar Cap: A Review

Keisuke Hosokawa<sup>1</sup> · Anita Kullen<sup>2</sup> · Steve Milan<sup>3</sup> ·  
Jade Reidy<sup>4,5</sup> · Ying Zou<sup>6</sup> · Harald U. Frey<sup>7</sup> ·  
Romain Maggiolo<sup>8</sup> · Robert Fear<sup>4</sup>

Received: 30 April 2019 / Accepted: 23 January 2020  
© The Author(s) 2020

**Abstract** This paper reviews our current understanding of auroral features that appear poleward of the main auroral oval within the polar cap, especially those that are known as Sun-aligned arcs, transpolar arcs, or theta auroras. They tend to appear predominantly during periods of quiet geomagnetic activity or northwards directed interplanetary magnetic field (IMF). We also introduce polar rain aurora which has been considered as a phenomenon on open field lines. We describe the morphology of such auroras, their development and

---

Auroral Physics

Edited by David Knudsen, Joe Borovsky, Tomas Karlsson, Ryuho Kataoka and Noora Partmies

---

✉ K. Hosokawa  
[keisuke.hosokawa@uec.ac.jp](mailto:keisuke.hosokawa@uec.ac.jp)

A. Kullen  
[kullen@kth.se](mailto:kullen@kth.se)

S. Milan  
[steve.milan@leicester.ac.uk](mailto:steve.milan@leicester.ac.uk)

J. Reidy  
[jr10g11@soton.ac.uk](mailto:jr10g11@soton.ac.uk)

Y. Zou  
[yz0025@uah.edu](mailto:yz0025@uah.edu)

H.U. Frey  
[hfrey@ssl.berkeley.edu](mailto:hfrey@ssl.berkeley.edu)

R. Maggiolo  
[romain.maggiolo@aeronomie.be](mailto:romain.maggiolo@aeronomie.be)

R. Fear  
[R.C.Fear@soton.ac.uk](mailto:R.C.Fear@soton.ac.uk)

<sup>1</sup> Dept. of Comm. Engineering and Informatics, Univ. of Electro-Communications, Tokyo, Japan

<sup>2</sup> Space and Plasma Physics, School of Electrical Engineering and Computer Science, KTH Royal Institute of Technology, Stockholm, Sweden

<sup>3</sup> Dept. of Physics and Astronomy, University of Leicester, Leicester, UK

<sup>4</sup> Dept. of Physics and Astronomy, University of Southampton, Southampton, UK

dynamics in response to solar wind-magnetosphere coupling processes, and the models that have been developed to explain them.

**Keywords** Polar cap aurora · Transpolar arc · Sun-aligned arc · Polar rain aurora · Ionospheric convection · Magnetosphere · Reconnection

## 1 Introduction

### 1.1 Transpolar Arc or Theta Aurora

The first report of auroral arcs appearing poleward of the main oval stem from the early 19th century (Mawson 1916, 1925). In the 1970s polar cap arcs were examined more systematically with the help of ground-based cameras. These observational studies revealed that polar cap arcs are typically thin, Sun-aligned auroral arcs that occur nearly exclusively during quiet times (e.g., Ismail et al. 1977; Lassen and Danielsen 1978). The first global images of the auroral oval from high-altitude became available in the early 1970s. High-altitude space-based observations have the advantage that the whole polar cap can be seen at once and long duration observations of the same feature are possible. High altitude observations have to be done in the ultraviolet (UV) because observations in visible light would severely suffer from the large brightness difference between the dark nightside and the bright dayside. High-altitude observations started with a scanning photometer onboard the ISIS-II satellite in the early 1970s. However, the global structure of polar arcs was not understood until the 1980s when the Spin-scan Auroral Imaging (SAI) UV photometer onboard DE-1 (Dynamics Explorer 1: Frank et al. 1981) and later-on a UV imager onboard the Viking satellite produced instant images with a (near) global view of the oval. The SAI UV photometer onboard DE-1 was also the instrument that for the first time provided observations of small-scale polar cap arcs, which will be introduced in Sect. 1.2, and allowed an investigation of the auroral distribution, current systems, and convection electric fields (Frank et al. 1982). When the first global auroral images from DE-1 were taken, it became clear that much larger auroral structures may appear in the quiet-time polar cap. Frank et al. (1982, 1986) published DE-1 images where 1000–1500 km-long Sun-aligned auroral arcs span the entire polar cap and connect the nightside to the dayside oval (see Fig. 1, left plot). Due to the resulting theta-shape of the global auroral pattern, Frank et al. (1982) suggested the name “theta aurora” for this phenomenon. Further progress was made in the 1990s–2000s with the Polar UVI (Ultraviolet Imager: Torr et al. 1995) and IMAGE (Imager for Magnetopause-to-Aurora Global Exploration) FUV (Far-Ultraviolet) instruments (Mende et al. 2000) that provided true 2-dimensional imaging in different wavelengths, which allowed the estimation of the mean precipitation electron energy and the distinction between electron and proton aurora, respectively. Due to the high temporal resolution of Polar and IMAGE (producing UV images at a 2-min cadence) the temporal evolution of large-scale polar arcs could be studied in much more detail than with previous instruments. A large number of observations of large-scale transpolar arcs reported in this section were obtained by these two instruments.

<sup>5</sup> British Antarctic Survey, Natural Environment Research Council, Cambridge, UK

<sup>6</sup> Dept. of Space Science, University of Alabama in Huntsville, Huntsville, USA

<sup>7</sup> Space Sciences Laboratory, University of California Berkeley, Berkeley, CA, USA

<sup>8</sup> Belgian Institute for Space Aeronomy, Brussels, Belgium

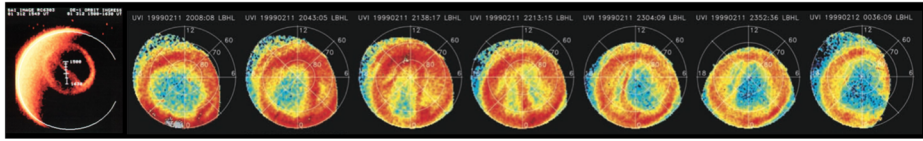


**Fig. 1** (left) DE-1 image of a transpolar arc forming a true theta aurora in the northern polar cap (from Frank et al. 1986); (right) Time sequence of Polar UV images in CGlat coordinates showing a TPA that forms at dawn and moves over the entire polar cap until it reaches the dusk oval side. Note, a smaller duskside oval-aligned TPA appears simultaneously (from Kullen et al. 2002)

Nowadays, the expression ‘transpolar arc’ (TPA) is more commonly used for that type of large-scale polar arc than ‘theta aurora’. By definition, a true theta aurora spans the polar cap from midnight to noon. However, this is not always the case during the arc’s entire lifetime. Often, a TPA starts to form at the dawn or duskside oval before it moves poleward and becomes a true theta aurora (Cumnock et al. 1997). Thus, the oval resembles the Greek letter theta only during part of a TPA’s several-hour-long lifetime (average lifetime of 2 hours according to Kullen et al. 2002). In rare cases TPAs move even over the entire polar cap until they reach the opposite side of the oval (Huang et al. 1989; Cumnock et al. 2002; Kullen et al. 2002; Cumnock 2005). An example of such a dawn-dusk moving TPA is shown in Fig. 1, right plot. However, most TPAs never become true theta auroras; those which form close to the dawn- or duskside oval often remain there. Such TPAs are also referred to as oval-aligned arcs (Murphree and Cogger 1981; Elphinstone et al. 1990; Kullen et al. 2002). TPAs are in general rare events, they are visible on auroral images during only 10–16% of the time (Kullen et al. 2002). Those TPAs which show a considerable dawn-dusk motion are even less common (15% of all TPAs according to Kullen et al. (2002), and 24% according to Fear and Milan (2012a)).

On rare occasions (7% of all TPAs according to Kullen et al. 2002), a TPA starts to form at the nightside oval and stretches from there into the empty polar cap. Such nightside-originating arcs have occasionally been reported (Craven et al. 1986; McEwen and Zhang 2000; Kullen et al. 2002; Milan et al. 2005; Goudarzi et al. 2008; Fear and Milan 2012b). Nightside-originating TPAs often evolve at the end of substorm recovery from a bulge at the poleward boundary of a typically thick oval and stretch towards noon. At the time of formation such TPAs are often more patchy than the usually thinner Sun-aligned TPA. Recovery oval bulges that reach far into the polar cap do not always develop into TPAs that stretch all the way to noon but collapse after a while (Kullen et al. 2002; Goudarzi et al. 2008).

There exist numerous reports about TPAs that deviate in formation and motion from the most typical TPA evolution. For example, Eriksson et al. (2005) showed a TPA case where the dayside part is split in two branches. Sometimes, oval-aligned arcs appear simultaneously on both oval sides, causing an oval shape that resembles the so-called horse-collar oval (Hones et al. 1989)—the region between oval-aligned arc and oval is in such cases typically filled with small-scale arcs, see Sect. 1.2. On other occasions, one TPA moves poleward while the TPA on the other oval side remains static (see Fig. 1, right plot). That two TPAs appear simultaneously, is not uncommon, this happens during about 30% of all TPA events (Kullen et al. 2002). Although TPAs are generally Sun-aligned, occasionally their tailward end becomes (during part of their lifetime) strongly hook-shaped (Ismail and Meng 1982; Murphree et al. 1982; Gusev and Troshichev 1986). This should not be confused with bending arcs (Kullen et al. 2002). The bending arcs are typically faint polar cap arcs where the dayside tip of the arc splits from the oval and moves successively antisunward, while the

tailward arc end remains attached to the oval, until the entire arc is strongly curved before disappearing within 10 s of minutes (Kullen et al. 2015; Carter et al. 2015).

Sometimes, the polar cap is filled with multiple polar cap arcs that evolve in a seemingly unordered manner, both from the dawnside, duskside as well as the nightside oval boundaries (Newell et al. 1999; Kullen et al. 2002). Observations in the last decade from UV imagers on low-orbiting satellites (they have a better resolution but not a full global view on the oval) revealed that multiple arc events are far more common than previously anticipated. During extended periods of northward IMF the entire polar cap may in rare cases even disappear completely (Zhang et al. 2009). Zhang et al. (2016) showed that multiple arcs are rather ‘cusp-aligned’ than sun-aligned, as their dayside ends are connected to the cusp, one of these cusp-aligned events (an example of such cusp-aligned multiple arcs will be shown later in Fig. 13a in 2.3). Possible explanations for that behavior are discussed in Sect. 2.3. Multiple ion beams appearing several Earth radii above the polar cap (Maggiolo et al. 2006, 2011) have been shown to be the high-altitude signatures of multiple polar cap arcs (Maggiolo et al. 2012). These are described in more detail in Sect. 3.4.

The disadvantage of most global auroral imagers is their poor spatial resolution (e.g. 1 pixel corresponds to 35–50 km in Polar UVI) and low luminosity sensitivity, making it difficult to identify small-scale Sun-aligned arcs or any TPA fine structure. With help of simultaneous ground-based cameras (Feldstein et al. 1995) and particle detectors (Makita et al. 1991; Cumnock et al. 2009) it was shown that a TPA appearing often as one 50–300 km wide structure on a satellite image from DE-1, Polar, or IMAGE, consists in reality of multiple thin auroral arcs. Due to the lower luminosity sensitivity of global imagers, another problem occurs: even when a TPA seems to be far inside the polar cap on a global image (i.e., the arc is clearly separated by a dark region from the main oval on the image) it is often still attached to the oval by (in the image) subvisual particle precipitation regions, as pointed out by Newell et al. (2009) (e.g. Fig. 2, right plot). However, at least those TPAs that start to form as oval-aligned arcs, but then move over the entire polar cap to the opposite oval side will at some point become completely separated from the oval side they came from (see Fig. 2). Thus Newell et al.’s (2009) categorization into oval-aligned TPAs (that are attached to the oval) and true theta aurora does not make much sense for TPAs that have such an evolution. A TPA like the ones shown in Figs. 1 and 2 would at the beginning of its lifetime belong to the category ‘oval aligned TPA’ while when reaching the noon-midnight meridian the same TPA would be classified a ‘true theta aurora’.

As discussed in detail in the excellent review by Zhu et al. (1997), studying polar cap arcs from ground-based cameras (where the large-scale auroral pattern remains unclear due to the limited field of view), and space based global auroral imagers (where small-scale Sun-aligned arcs remain subvisual due to low resolution and high luminosity threshold), resulted in sometimes contradicting results regarding particle characteristics and source regions of polar cap arcs. Zhu et al. (1997) suggested that part of the confusion appears because small-scale Sun-aligned arcs and TPA probably have different source regions. For small-scale Sun-aligned arcs it was for a long time unclear whether they appear on open or closed field lines (e.g. Bonnell et al. 1999), however more recent results point again to an open field line source region (see Sect. 3.3 and 5.2 for further details). The studies from the 1980s and 1990s focusing on large-scale TPAs all pointed to the plasma sheet or its boundary layer as the origin, due to slightly lower particle energies, but otherwise with similar particle characteristics as auroral arcs of the main oval (e.g., Frank et al. 1986; Peterson and Shelley 1984).

Further indication that TPAs map to the plasma sheet is the fact that these seem to lie on closed field lines. The most direct evidence stems from Fear et al. (2014), who showed

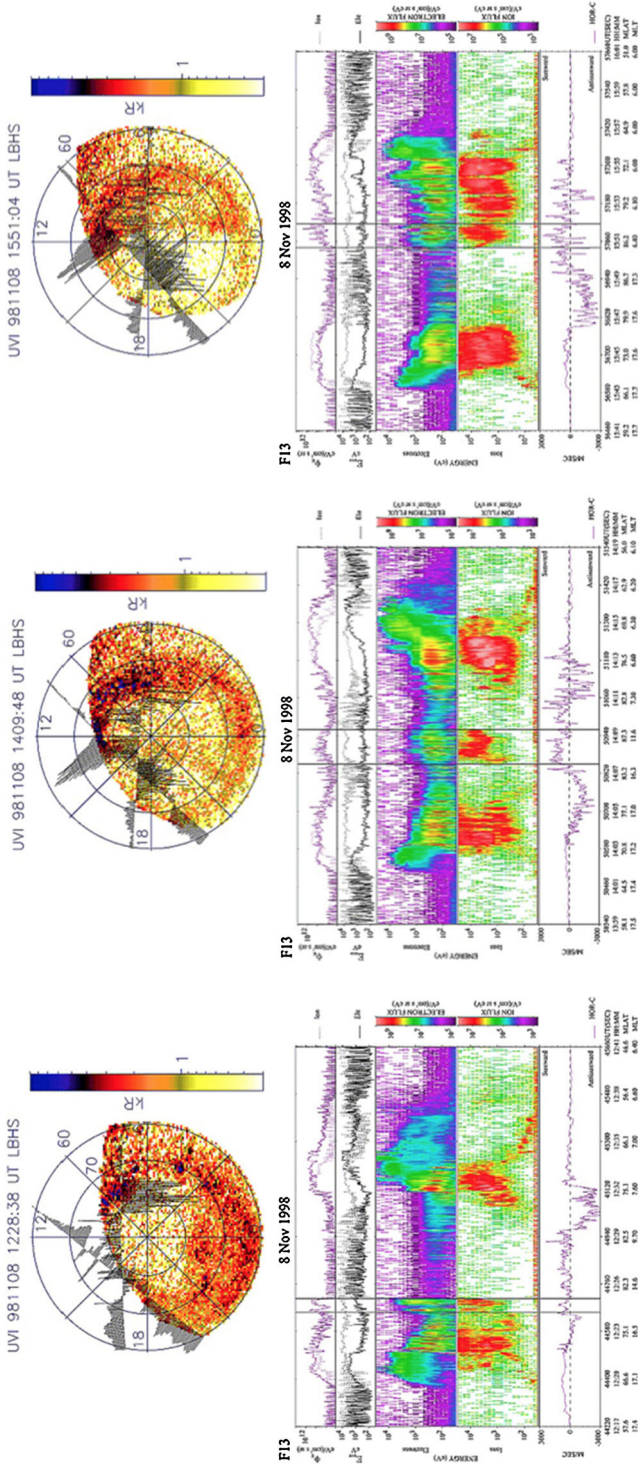
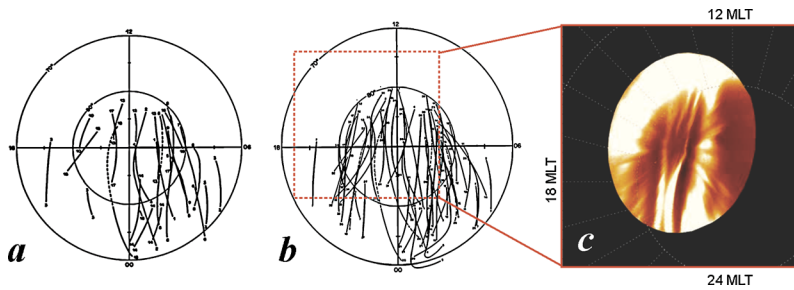


Fig. 2 DE-1 images and DMSP particle data from a TPA that forms at the dusk oval and moves subsequently over the entire polar cap until it reaches the dawn oval side. On the left image, particle data show that the TPA is still attached to the dusk side, on the right image it has merged with the dawn side oval (figures from Cummoek et al. 2002)



**Fig. 3** (a) Collection of small-scale Sun-aligned arcs (taken from Berkey et al. 1976). (b) Similar statistical collection of the arcs (taken from Ismail et al. 1977). (c) Example of ground-based all-sky image of small-scale Sun-aligned arcs obtained by an all-sky cooled CCD imager at Resolute Bay

observations of double-loss cone electrons in the magnetotail mapping to a TPA. Another indication for closed field lines is the observed TPA conjugacy. There exist many reports that TPAs are a conjugate phenomenon appearing simultaneously in the northern and southern hemispheres on opposite oval sides and moving in opposite directions (e.g., Mizera et al. 1987; Obara et al. 1988; Huang et al. 1989; Craven et al. 1991; Cumnock et al. 2006; Carter et al. 2017; Xing et al. 2018). However, Østgaard et al. (2003) showed that during certain IMF  $B_x$  conditions, a clear TPA appears only in one hemisphere (see Sect. 3.6 for more details). That TPAs appear within sunward plasma flow in the polar cap was taken as further evidence for a plasma sheet source (e.g., Meng 1981; Peterson and Shelley 1984; Frank et al. 1986; Frank and Craven 1988; Huang et al. 1987, 1989). However, as Liou et al. (2005) pointed out, these studies were all based on satellite measurements from the dayside polar cap. Their own observations, and those of Nielsen et al. (1990) showing anti-sunward flows along the nightside part of TPAs let them suggest that (at least the nightside part of a) TPA may map to the LLBL (Low-Latitude Boundary Layer) at the flanks. A large part of this review is dedicated to the still ongoing discussion about the origin of TPAs. For a more general survey of the magnetosphere's behavior during periods of northward IMF, we refer the interested reader to a recent review by Fear (2019).

## 1.2 Sun-Aligned Arcs and Horse-Collar Aurora

As mentioned in the previous section, larger and brighter arcs in the polar cap region are traditionally called 'theta aurora' or 'transpolar arcs'. Such large-scale arcs have been observed by several space-based optical instruments onboard DE-1, Polar, and IMAGE. In contrast, small and relatively dim (subvisible in most cases) arcs have been observed by ground-based optical instruments. The morphology of such small-scale arcs was studied intensively in the 70's and early 80's by using ground-based intensified photometers located in the polar cap (e.g., Lassen 1972; Ismail et al. 1977) and since then they have been known as 'Sun-aligned arcs'. It was also indicated that such small-scale sub-visual Sun-aligned arcs are present in the polar cap more often than is implied by space-based data (Weber and Buchau 1981). Figures 3a and 3b show collections of Sun-aligned arcs detected by one of the earlier studies (Berkey et al. 1976; Ismail et al. 1977). One end of the arcs is directed to the Sun, which is the reason why small-scale arcs in the polar cap are called 'Sun-aligned arcs.' In the 70's or 80's, people already knew that the small-scale Sun-aligned arcs are indeed a northward  $B_z$  phenomenon. Since then, Sun-aligned arcs have been studied extensively by combining space-based and ground-based instruments and such earlier observations up to the late 90's

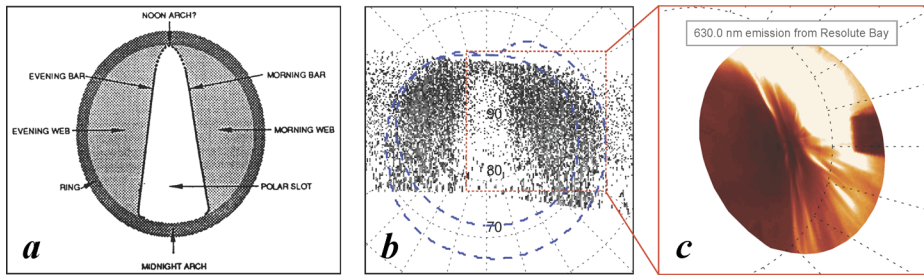


**Fig. 4** (a) Schematic illustration of horse-collar aurora during northward IMF condition (taken from Hones et al. 1989). (b) Space based optical observations from DMSP SUSSI instrument on January 6, 2013. (c) Simultaneous ground-based 630.0 nm optical observations from an all-sky imager at Resolute Bay, Canada

are summarized in the review of Zhu et al. (1997). After Zhu et al. (1997), highly-sensitive all-sky imagers have been employed to observe weak Sun-aligned arcs (e.g., Hosokawa et al. 2011). An example of the 630.0 nm red line emission is shown in Fig. 3c. A few thin arcs traversing the field-of-view from the bottom to the top are the manifestations of Sun-aligned arcs. In addition to such a large-scale structure of the arcs, small radially aligned features are embedded within the arcs, which are internal substructures of the arcs representing their extension in the direction of altitude. These substructures are not associated with the Sun-aligned elongation of the arcs.

During periods of prolonged northward IMF conditions, the polar cap boundaries on the duskside and dawnside move poleward to form a large-scale configuration known as “horse-collar aurora” (Hones et al. 1989). Figure 4a is a schematic illustration from Hones et al. (1989), in which the light grey region is a region of soft particle precipitation called ‘web’. Figure 4b is a space-based optical observation from the SUSSI (Special Sensor Ultraviolet Spectrographic Imager) instrument onboard the Defense Meteorological Satellite Program (DMSP) satellite. The shape is similar to the cartoon shown in Fig. 4a. If we look at the dawnside part of the collar (Fig. 4c), by using highly-sensitive ground-based all-sky camera, the morning web of the horse collar aurora is composed of a number of small-scale Sun-aligned arcs. That is, small-scale Sun-aligned arcs and horse collar aurora geometry are closely associated with each other, which is consistent with the fact that the most frequently occurring polar cap arcs are the arcs confined either in the morning sector or the evening sector of the polar cap (e.g., Zhu et al. 1996).

### 1.3 Polar Rain Aurora

Aurora and particle precipitation occurring in the polar cap are naturally associated with each other. Weak, uniform, electron precipitation, known as polar rain, has been found to be present across the entire polar cap both, during southward and northward IMF conditions (Winningham and Heikkila 1974). This kind of precipitation originates in the solar wind and enters the ionosphere via open field lines (Baker et al. 1986). Hardy et al. (1982) reported polar cap arcs embedded within polar rain, which led them to suggest the arcs themselves were occurring on open field lines.

Structured, localized precipitation, known as polar showers, interrupts the soft electron precipitation during northward IMF (Hardy 1984; Hardy et al. 1986). Shinohara and Kokubun (1996) classified two different types of polar showers using one year of particle data from a Defense Meteorological Satellite Program (DMSP) spacecraft. The first

(‘type A’) is associated with ion flux; the second (‘type B’) is not. The type A polar showers were found to be more intense than type B. Furthermore, type A showed no dependence on the IMF  $B_x$  or  $B_y$  components whereas type B demonstrated a statistically similar dependence on the IMF condition to typical polar rain. For example, the type B polar showers occurred predominantly in the northern hemisphere for negative IMF  $B_x$  and in the southern hemisphere for positive IMF  $B_x$ , as does polar rain (Yeager and Frank 1976; Meng and Kroehl 1977). This led Shinohara and Kokubun (1996) to suggest that the properties of the type A polar showers are similar to plasma sheet boundary layer plasma and hence occur on closed field lines, whereas the type B polar showers have similar properties to the solar wind and hence occur on open field lines. Type A polar showers are suggested to be linked with large-scale theta aurora (e.g. Frank et al. 1982), discussed in Sect. 1.1. However, as discussed above, theta auroras are known to have a dependence on the IMF  $B_y$  component whereas the type A polar showers were found to be independent of IMF  $B_y$  and  $B_x$ . This apparent discrepancy can be attributed to Shinohara and Kokubun (1996) using the instantaneous IMF conditions instead of accounting for the time for the IMF  $B_y$  to propagate into the magnetotail. This propagation time was discussed by Fear and Milan (2012a), who found a 1–3 hour time delay (dependent on solar wind conditions) in the correlation between IMF  $B_y$  and the position where transpolar arcs form in the polar cap.

One of the key questions surrounding polar cap arcs occurring on open field lines is whether they result from accelerated polar rain, and if so, what is the acceleration mechanism? Carlson and Cowley (2005) addressed this question by assuming the source region of polar cap arcs to be polar rain and then estimated several electrodynamic parameters using kinetic theory. They found good agreement between their estimates and observations of polar cap arcs from Carlson et al. (1988). Their analysis indicates that polar cap arcs are produced by field-aligned acceleration of polar rain electrons. Carlson and Cowley (2005) state that any modest mechanism that drives shear flows across open field lines could cause this acceleration, for example at the boundaries between the ‘lobe’ cells and ‘merging’ cells. The authors state that they expect polar cap aurora caused by accelerated polar rain to be present whenever the IMF is northward, which is approximately half the time.

It has been suggested that polar cap arcs occurring on open field lines, consistent with accelerated polar rain, can be identified by electron-only particle precipitation. This was discussed by Newell et al. (2009) in a review of polar cap precipitation and aurora. They argue that weaker Sun-aligned arcs are distinct from the large-scale transpolar arcs that occur on closed field lines (discussed in Sect. 1.2). Reidy et al. (2017) observed a Sun-aligned arc associated with electron-only precipitation, using particle data and conjugate UV images of the aurora from a DMSP spacecraft. Several aspects of this arc were consistent with observed dependencies for polar rain, namely it occurred on the duskside of the northern hemisphere during negative  $B_x$  and positive  $B_y$  conditions. These properties are similar to the ‘type B’ polar showers found by Shinohara and Kokubun (1996). Reidy et al. (2017) concluded, using these observations combined with the electron-only precipitation, that this arc was consistent with formation on open field lines. Figure 5, taken from the Reidy et al. (2017) survey, shows an observation of polar cap arcs associated with different types of particle precipitation occurring in the same auroral UV image. The corresponding particle data (right) shows the precipitation measured as the spacecraft crossed the polar cap. The red lines in both the auroral image and particle spectrogram indicate when the spacecraft sampled a polar cap arc associated with ion and electron precipitation, consistent with the type A polar showers; the orange lines show the spacecraft measuring a polar cap arc associated with electron-only particle precipitation, consistent with the type-B polar showers. These ‘electron-only’ arcs were found to be consistent with accelerated polar rain, as proposed by Carlson and



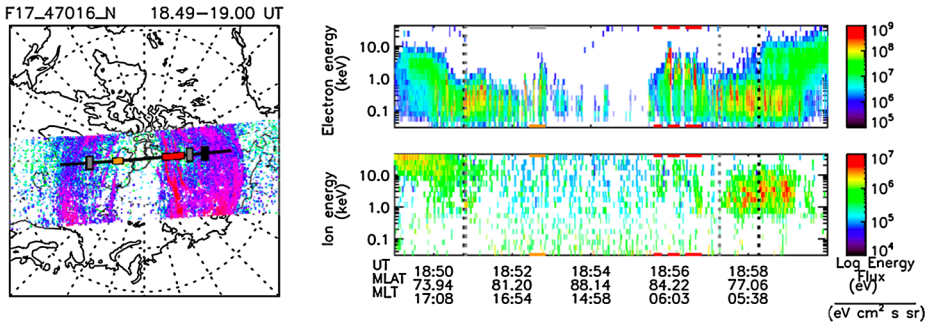


**Fig. 5** UV image from the SSUSI instrument (left) with the corresponding particle measurements from SSJ/5 (left) onboard DMSP F17 taken between 18:49–19:00 UT on 15 December 2015 (taken from Reidy et al. 2017). The black line in the SSUSI image represents the footprint of the DMSP spacecraft. The orange and red lines on the footprint and in the particle spectrogram correspond to electron-only and electron and ion signatures within the polar cap respectively, these features were identified from the particle spectrogram and can be seen to coincide with polar cap arcs in the SSUSI images

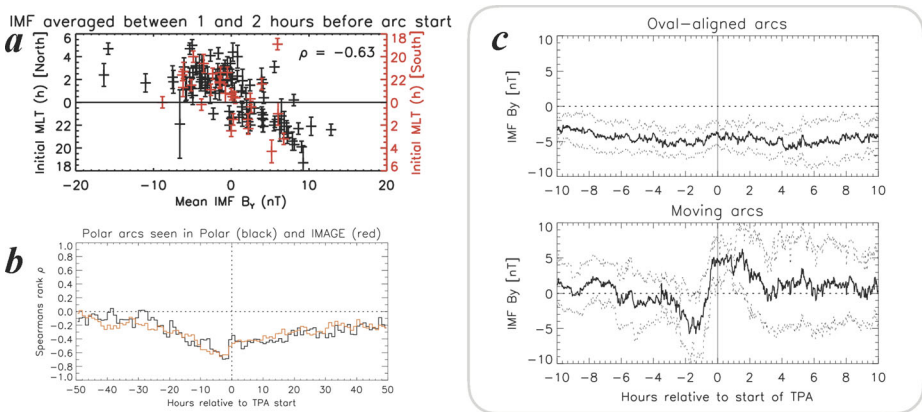


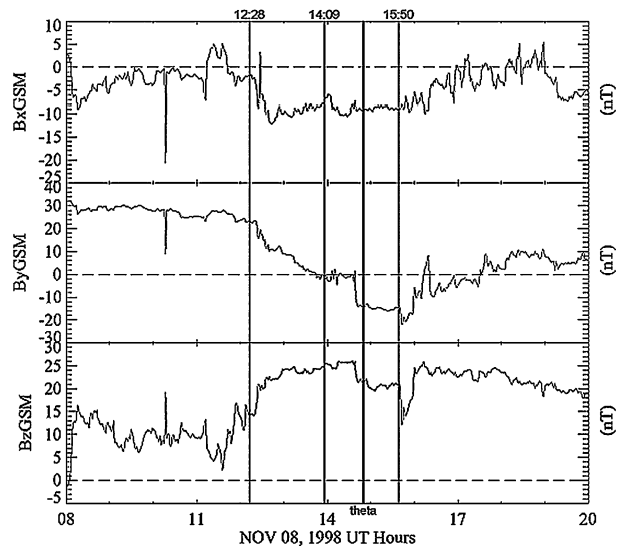
**Fig. 6** (a) IMF  $B_y$  1–2 h before TPA formation versus MLT location of TPA intersection with the nightside oval (Fear and Milan 2012a), (b) correlation between initial arc location and hourly average IMF  $B_y$  up to  $\pm 50$  h from TPA formation for Kullen et al.'s (2002) (black curve) and Fear and Milan's (2012a) (red curve) TPA datasets, (c) Superposed epoch analysis plot of IMF  $B_y$  up to  $\pm 10$  hours from TPA formation, centered at TPA start time. The sign of IMF  $B_y$  is reversed for all arcs that form on the dusk oval side (Kullen et al. 2015)

Cowley (2005). However, Reidy et al. (2018) did speculate, in this case, that the lack of ion precipitation could be due to instrument sensitivity. Further work is needed to fully understand these polar-rain-accelerated arcs and what exactly is causing them.

### 1.4 IMF Dependence of TPAs

It has been known for several decades that both small-scale Sun-aligned arcs (Valladares et al. 1994) and TPAs are a predominantly northward IMF phenomenon, while IMF  $B_y$  controls their location and motion (e.g., Gussenhoven 1982; Frank et al. 1986; Elphinstone et al. 1990). Most duskside TPAs appear during duskward IMF conditions, most dawnside TPAs during dawnward IMF in the northern hemisphere (Elphinstone et al. 1990; Kullen

**Fig. 7** IMF conditions for the dawn-duskward moving TPA shown in Fig. 2. The vertical bars mark the points of time for which the three images are shown in Fig. 2. The vertical lines have been shifted 15 min to account for the time delay between the Wind satellite at  $X = +75 R_E$  and  $X = 0 R_E$  (figure from Cumnock et al. 2002)



et al. 2002). Fear and Milan (2012a) showed that the statistical dependence of TPA location and formation on IMF  $B_y$  is even more exact. There is a clear correlation between IMF magnitude and MLT location of the initial nightside oval intersection when a TPA starts to form. As can be seen in Fig. 6a, this is only statistically correct. Some (especially dawnside) TPAs form on the ‘wrong’ oval side for a certain IMF  $B_y$  value, often in connection with the simultaneous appearance of another TPA on the ‘correct’ oval side (Hones et al. 1989; Elphinstone et al. 1990; Kullen et al. 2002). Much confusion about the IMF dependence of TPAs stems from the fact that we do not know the exact time delay between IMF conditions and their effect on TPA location. In many studies with varying IMF  $B_y$  and  $B_z$ , the time of TPA formation was compared to concurrent IMF conditions, which resulted in partially incorrect conclusions. Fear and Milan (2012a) and Kullen et al. (2015) showed with independent TPA datasets, that the time delay is at least 1–2 hours. As shown in Fig. 6b, the correlation between IMF  $B_y$  and initial TPA location is high even for  $B_y$  values several hours before the TPA forms. The time delay cannot be determined more exactly, as most TPAs (visible in global images) appear during times with strong IMF. Kullen et al. (2002) showed that TPAs form preferably during solar wind conditions with a high magnetic energy flux  $v \times B^2$  and strong northward IMF (Kullen et al. 2002), probably due to the reported correlation between magnetic energy flux and TPA luminosity in the dayside polar cap (Kullen et al. 2008). Such solar wind conditions appear typically during CMEs or similar events, where the IMF magnitude is large, and the IMF components remain more or less constant during several hours. This explains the nearly constant average IMF  $B_y$  values during the hours around oval-aligned TPAs, as seen in Polar UV statistics (Kullen et al. 2015) and shown in Fig. 6c (top).

A connection between the poleward motion of TPAs, and an IMF  $B_y$  sign reversal was first discovered by Cumnock et al. (1997). A duskside TPA in the northern hemisphere will move over the polar cap towards dawn after IMF  $B_y$  has changed sign from duskward to dawnward, see the TPA example shown in Fig. 2 and corresponding IMF data in Fig. 7. For an opposite sign change, a dawnside TPA is expected to move towards dusk. Cumnock (2005) showed with a statistical study that one clear IMF  $B_y$  sign change during constantly northward IMF is a sufficient condition for a poleward motion of a TPA to occur, as long

as the solar wind magnetic energy flux is high enough (Kullen et al. 2008). The different examples discussed in Kullen et al. (2002) and Cumnock (2005) show that TPAs that move over the entire polar cap to the other oval side require an IMF  $B_y$  sign reversal, while for TPAs reaching only the center of the polar cap, an IMF  $B_y$  magnitude decrease is sufficient. Cumnock's (2005) observations that 16 of the 19 TPAs in her study had already formed before an IMF  $B_y$  sign change took place, shows, that an IMF  $B_y$  sign change does not necessarily trigger the TPA formation itself (as originally assumed by, e.g. Chang et al. (1998) or Kullen (2000)) but only its subsequent motion in direction of IMF  $B_y$ . This can also be seen from Fig. 6c (bottom), where an IMF  $B_y$  sign change appears on average 40 min before a moving TPA forms, which is clearly shorter than the at least 1–2 hours time delay required for IMF  $B_y$  to affect the TPA location at formation (Fear and Milan 2012a, Kullen et al. 2015).

So far, the IMF  $B_y$  effect has been discussed only for TPAs in the northern hemisphere. From the observational reports of conjugate TPAs appearing in the northern and southern hemisphere on opposite oval sides and with opposite motion (see Sect. 1.1 for references), it can be inferred that IMF  $B_y$  has an opposite effect on TPA location and motion in the southern hemisphere. However, the interhemispheric TPA conjugacy may be prevented by a strong IMF  $B_x$  component. Several statistical studies show a (weak) correlation between IMF  $B_x$  and the occurrence of high-latitude aurora in general. TPAs (Kullen et al. 2002), small-scale polar arcs (Lassen and Danielsen 1978), and also localized High-Latitude Day-side Aurora (HiLDA) (Frey 2007 and references therein), are in the northern hemisphere more commonly observed during negative than during positive IMF  $B_x$ . The conjugacy issue and its connection to IMF  $B_x$  is discussed in more detail in Chap. 3.6 in connection with a discussion of non-conjugate TPA cases observed by Østgaard et al. (2003).

## 2 Proposed Generation Models

### 2.1 IMF $B_y$ Switching for TPA

The reason why a TPA forms has been discussed extensively in the last decades. As described in detail in Kullen's (2012) review about large-scale TPAs, there exist many different models trying to explain their cause. Most of these models are conceptual, and are based on observations of IMF control of TPAs. The IMF dependence of TPA formation and motion is already described in Sect. 1.4. In the present chapter, the different TPA models are presented. Many TPA models focus on the topological connection between TPAs and the tail plasma sheet, as the plasma sheet or its boundary region is generally believed to be the source region of TPAs (see Sect. 1.1 and 5.2 for more details). Meng (1981) proposed that an oval-aligned TPA appears on the poleward boundary of an expanded closed field line region. Makita et al. (1991) suggested among other ideas, that the poleward expansion of the closed field line region is caused by a tail configuration where the entire plasma sheet is twisted around the  $x$ -axis, such that one plasma sheet flank appears on very high latitudes and the other on much lower. This is shown in Fig. 8b (see also Sect. 2.4 where this model is discussed again in connection with small-scale Sun-aligned arcs). Such a tail twist appears indeed for nonzero IMF  $B_y$  (see Fig. 8a), as first proposed by Cowley (1981) and later on confirmed both observationally (Kaymaz et al. 1994; Owen et al. 1995; Tsyganenko and Fairfield 2004) and with MHD (Magnetohydrodynamics) simulations (Walker et al. 1999; Kullen and Janhunen 2004). Tsyganenko et al.'s (2004) observational study as well as both MHD simulations showed that the degree of IMF  $B_y$ -induced tail twisting is much stronger

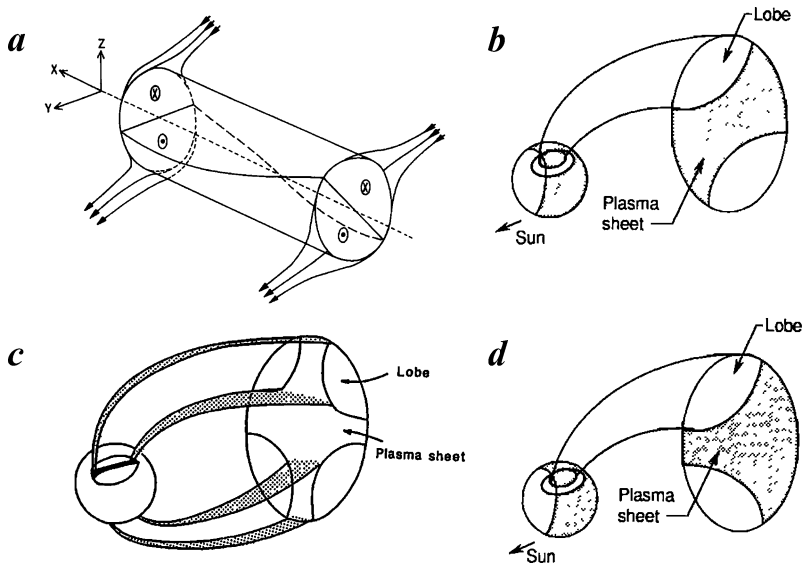


**Fig. 8** (a) Tail twist for duskward IMF (Cowley 1981) (b) oval-aligned TPA at dusk due to twist of tail plasma sheet for duskward IMF (Makita et al. 1991), (c) bifurcated tail plasma sheet mapping to a TPA in the center of the polar cap, and a conjugate TPA in the other hemisphere (Obara et al. 1988), (d) possible relations of polar cap arc formation with plasma sheet configuration (taken from Makita et al. 1991)

during northward than during southward IMF, which would explain why a considerable poleward expansion of the closed field line region (and thus the possibility of an oval-aligned TPA to form at its poleward boundary) appears only during northward IMF. With this simple model, it can be easily explained why oval-aligned TPAs appear typically at the dawnside oval during downward IMF and at the duskside oval during duskward IMF (see Sect. 1.4 for references), as well as why a conjugate TPA typically appears simultaneously in the southern hemisphere on the opposite oval side (see Sect. 1.1 for references about conjugate TPAs). Not explained with this model is, how exactly an oval-aligned TPA during fairly constant IMF  $B_y$  may become separated from the main oval. There, the tail reconnection during IMF northward non-substorm intervals (TRINNI) model by Milan et al. (2005) offers a possible explanation (see Sect. 2.2).

In the case that an oval-aligned TPA moves poleward and develops into a true theta aurora, the tail topology becomes more complicated. As already suggested by Frank et al. (1982, 1986) a TPA in the center of the polar cap should map to a plasma sheet filament that reaches from the main plasma sheet high into the lobe, such that the plasma sheet becomes bifurcated. A conjugate TPA will appear in the southern hemisphere that will map to a plasma sheet filament in the southern lobe (see Fig. 8c taken from Obara et al. 1988). As mentioned already in Sect. 1.1, such plasma filaments inside the lobe during TPA events have indeed been observed by e.g., Huang et al. (1989) and Fear et al. (2014).

As discussed in Sect. 1.4, a TPA moving over the entire polar cap is typically connected to an IMF  $B_y$  sign change. Thus, it can be expected that a  $B_y$  sign change from downward to duskward causes an originally clockwise-twisted plasma sheet to transform in an intermediate state into a bifurcated plasma sheet and finally into a new equilibrium state with an anti-clockwise twist for the new  $B_y$  direction. Kullen (2000) proposed that an IMF  $B_y$  sign change may cause such a tail reconfiguration, assuming that the tail will not change

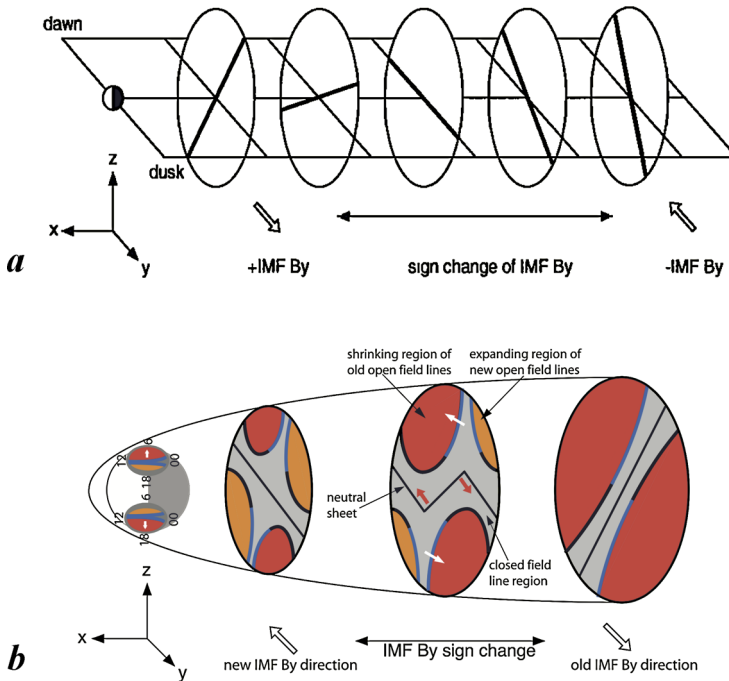


**Fig. 9** (a) Simple tail twist rotation model for an IMF  $B_y$  sign change by Kullen (2000), (b) tail topology after an IMF  $B_y$  sign change during northward IMF, as it appears in MHD simulations (from Kullen 2012)

its  $B_y$ -induced twist at once from e.g. clockwise to anti-clockwise, but with a time delay until far tail regions are affected. Thus, in an intermediate state, near-Earth and far tail regions are oppositely twisted (see Fig. 9a). By modifying the T89 model (Tsyganenko 1989) in such a way, Kullen (2000) showed, the closed field line region becomes indeed bifurcated in the near-Earth tail and maps to a finger of closed field lines in the polar cap. The closed field line finger moves from dawn to dusk while the tail rotation propagates tailward, as is expected for a TPA occurring for an IMF  $B_y$  sign change from negative to positive. MHD simulations with several different codes confirm in principle this scenario (Slinker et al. 2001; Maynard et al. 2003; Kullen and Janhunen 2004; Tanaka et al. 2004; Naehr and Toffoletto 2004). However, while the plasma sheet in Kullen (2000) was forced to stay straight while rotating (i.e. no bifurcation of the plasma sheet occurs), MHD results show that the reconfiguration does not only propagate tailward but also inward towards the tail center. As a result, the plasma sheet gets in an intermediate kinked (weakly bifurcated) state (see black line, indicating the neutral sheet in Fig. 9b). The MHD results are discussed in more detail in Sect. 4.1.

## 2.2 TRINNI for TPA

As discussed in Sect. 1.1., some large-scale TPAs appear to grow into the polar cap from the nightside auroral oval. The growth and evolution of one such event was studied in global auroral imagery (IMAGE) and global convection mapping (Super Dual Auroral Radar Network: SuperDARN, Chisham et al. 2007) of the northern hemisphere by Milan et al. (2005), a subset of the observations being presented in Fig. 10. Three snapshots of auroral imagery

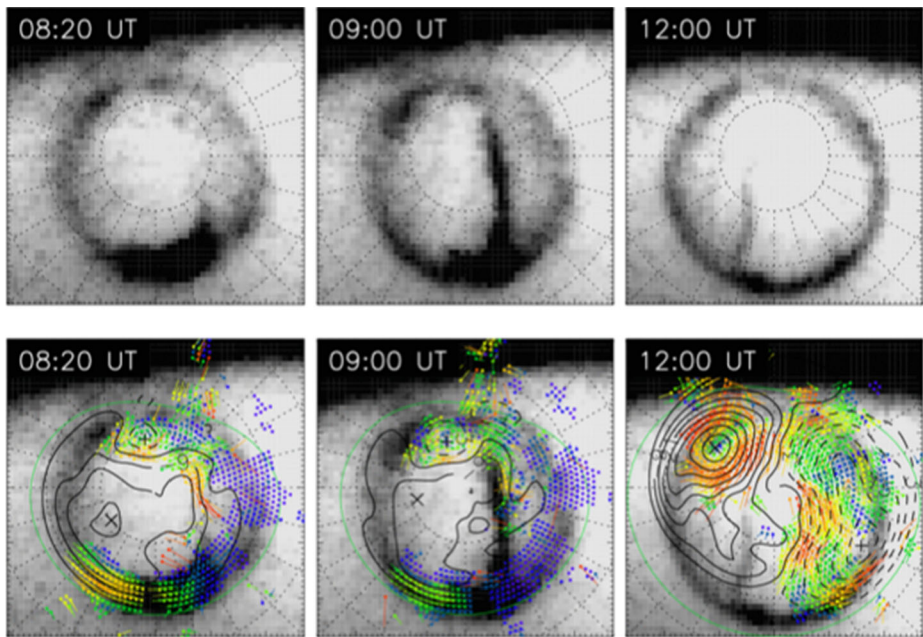


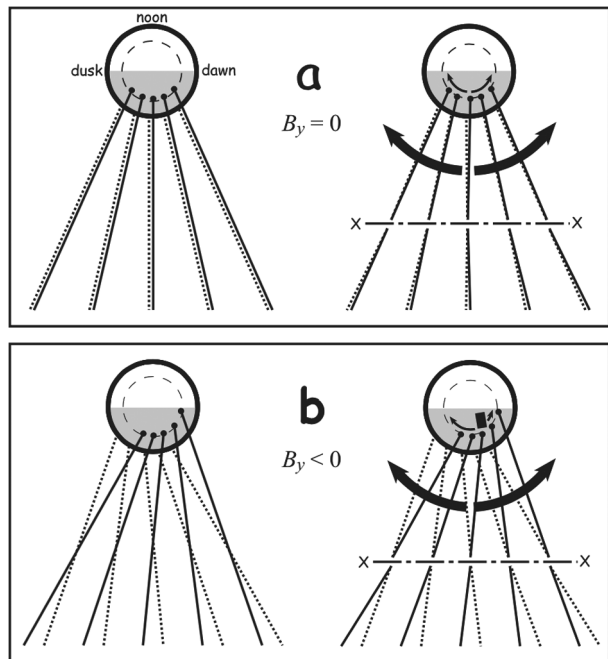
**Fig. 10** (Upper panels) Three auroral images captured by the Far Ultraviolet Wideband Imaging Camera (FUV-WIC) on the IMAGE spacecraft on 19 Jan 2002. (Lower panels) The same auroral images, with convection measurements by SuperDARN superimposed (after Milan et al. 2005)

from the Far Ultraviolet Wideband Imaging Camera (FUV-WIC) on the IMAGE spacecraft are shown from 08:20, 09:00, and 12:00 UT on 19 Jan 2002. They identified a modest brightening across the midnight sector of the auroral oval prior to the event and the development of a poleward intrusion into the polar cap of an auroral arc at the post-midnight edge of this brightening (left panel), followed by the subsequent growth of a TPA into the dawn-side portion of the polar cap (middle panel).

The convection observations showed that simultaneous to, and coincident with, the initial auroral brightening, occurring during a period of IMF  $B_z > 0$  and  $B_y < 0$ , fast westward ionospheric flows developed across the midnight sector, with much slower eastward flows to the east. Milan et al. (2005) noted that this distorted twin-cell return flow pattern was highly reminiscent of fast nightside flows that had been reported by Grocott et al. (2003, 2004) to occur during periods of prolonged northward IMF, and to have an east-west sense of flow that was determined by the  $B_y$  component of the IMF, and which was opposite in the northern and southern hemispheres. Such flow events have come to be known as tail reconnection during IMF northward non-storm intervals (TRINNI).

Grocott et al. (2003) had proposed a model for the formation of TRINNI that invoked the induction of a  $B_y$  component in the magnetotail lobe field by magnetic tension forces associated with magnetopause reconnection occurring during periods of northward but  $B_y$ -dominated IMF; reconnection of these lobe field lines by tail reconnection then leads to newly-closed field lines that are tilted out of meridional planes, leading to asymmetrical sunward return flows, with fast eastward or westward flow across the midnight meridian. The observations of Milan et al. (2005) suggested that the TPA initially formed close to the location where TRINNI return flows diverged eastward and westward. This led them

**Fig. 11** The model proposed by Milan et al. (2005) for the relationship between TRINNI occurrence and TPA formation. **(a)** With no  $B_y$  component in the tail, magnetotail field lines closed by reconnection are contained in meridian planes and can convect sunward. **(b)** With a  $B_y$  component, closed field lines are bent out of meridian planes, creating asymmetric return flows in the ionosphere as they convect sunwards, where the fast azimuthal flows across midnight are identified as the TRINNI; field lines crossing the equatorial plane near midnight have no easy sunward route and build up in the tail before protruding into the open polar cap



to speculate (see Fig. 11) that the TPA was formed by field lines which had undergone reconnection in the midnight sector of the tail and which consequently straddled the midnight meridian with footprints that were located in the dusk sector in one hemisphere and the dawn sector in the opposite hemisphere. They suggested that these field lines were unable to evolve back to the dayside in the convection return flow, accumulated in the midnight sector, and eventually protruded into the polar cap. The TPA was then formed by precipitation of trapped particles on these closed field lines.

The  $B_y$  component of the magnetic field in the lobe that leads to the formation of TRINNI, and by implication this class of TPAs, is created by reconnection at the magnetopause under conditions of significant IMF  $B_y$ . It might not be expected that field lines of one sense of  $B_y$  or another immediately impact the reconnection in the magnetotail, and promptly influence the east-west sense of the TRINNI flows. Fear and Milan (2012a) studied the time delay between periods of IMF of one east-west sense or the other and the control of the dawn-or-dusk sector formation of TPAs. They found that a delay of around 4 hours best explained their observations (see red curve in Fig. 6b), consistent with a reasonable estimate of the propagation time of newly-opened field lines to the tail reconnection site. A more recent study (Kullen et al. 2015) confirmed the overall trends found by Fear and Milan (2012a) but found the correlation peaked on a slightly shorter timescale (around 2 hours), see black curve in Fig. 6b. However, both studies are compatible with the TRINNI formation mechanism being responsible for at least a significant proportion of TPAs.

### 2.3 Instability for TPA

An alternative model to explain TPAs that form at the nightside oval and stretch from there sunward into the polar cap has been proposed by Rezhnev (1995) and in a slightly different variant by Golovchanskaya et al. (2006). Instead of invoking tail reconnection to explain the

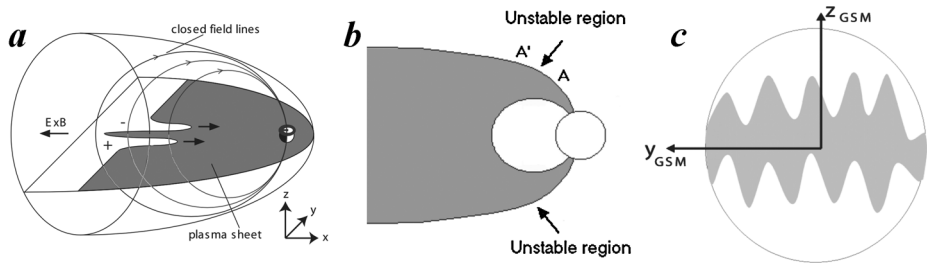


**Fig. 12** Interchange instability in strongly curved B-field region causing plasma filaments stretching into the lobes according to (a) Rezhenov (1995) and (b and c) Golovchanskaya et al. (2006). The filaments are assumed to map to nightside originating TPAs

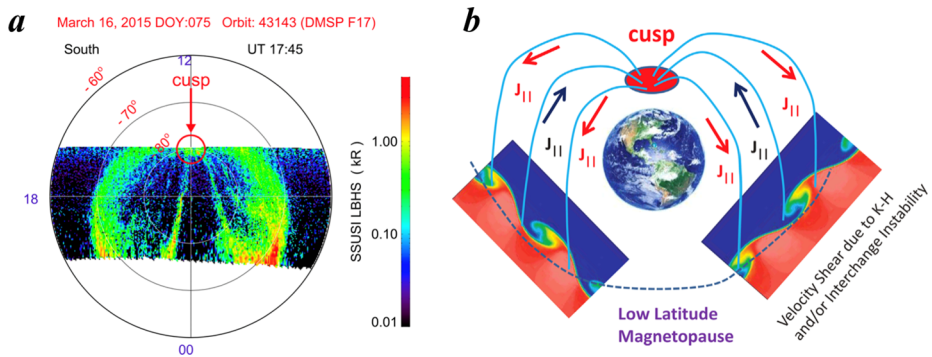


**Fig. 13** (a) Multiple cusp-aligned arcs seen in SSUSI LBHS images from the DMSF F17 satellite; (b) Model by Zhang et al. (2016) explaining the occurrence of multiple cusp-aligned arcs as a result of the Kelvin-Helmholtz instability occurring during northward IMF along the dayside magnetopause (Both Figures are taken from Zhang et al. 2016)

sunward growth of the TPA as in the conceptual model by Milan et al. (2005) described in Sect. 2.2., these authors showed with theoretical calculations that TPAs forming at the night-side oval may appear as a result of the ballooning instability acting on highly curved magnetic field lines. The instability causes the growth of plasma sheet filaments at the plasma sheet boundary into the lobes that would map to a sunward growing TPA. Note, this type of TPA model does not require a considerable IMF  $B_y$  component, as is the case in e.g., Kullen's TPA model (Kullen and Janhunen 2004) but needs solar wind conditions causing a strongly curved magnetic field, such as northward IMF, high solar wind speed and/or sub-storm recovery. Rezhenov (1995) suggested such an instability would appear at the tailward end of a short plasma sheet during northward IMF (resulting in a tailward-growing plasma sheet filament that would map to a sunward growing TPA, see Fig. 12a) while Golovchanskaya et al. (2006) located the instability at the strongly curved near-Earth part of the tail magnetic field lines (Fig. 12b), causing plasma sheet filaments to grow into the tail lobes. According to Golovchanskaya et al. (2006) this could also explain the emergence of multiple plasma sheet filaments (Fig. 12c), causing multiple nightside originating TPAs, as has been observed by e.g. Huang et al. (1989).

Zhang et al. (2016) suggested the Kelvin Helmholtz (KH) instability (which appears predominantly during northward IMF) and/or the interchange instability as a possible source of multiple polar arcs (see Fig. 13a). In their model, the instability appears along the low-



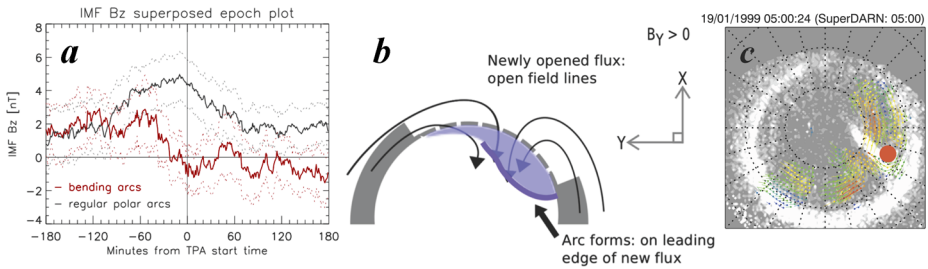


**Fig. 14** (a) Average IMF  $B_z$  up to 3 hours before and after formation of bending arcs (red) and regular TPAs (black); (b) bending arc model; (c) Polar UV image of bending arc overlaid by 10-min averaged SuperDARN plasma flows (figures from Kullen et al. 2015 and Carter et al. 2015)

latitude dayside magnetopause (see Fig. 13b for a schematic). Then the instability-generated waves lead to strong shear flows, which in turn may generate multiple field-aligned currents that map into the polar cap. Yamamoto and Ozaki (2005) suggested that this process is in principle possible by running a numerical model which produces dayside and polar cap arcs by FACs originating from the LLBL that is modulated by a KH-instability. As shown in Fig. 13b, plasma velocity shears exist on both sides of the open-closed field line boundary, thus some arcs may appear on open and other arcs on closed field lines. This would be one possible explanation for the open-closed field line issue of TPAs (see also 1.4 and 5.2). Zhang et al.'s (2016) model may explain the observed cusp-alignment of multiple polar arcs (see Fig. 13b) as well. However, the cusp-alignment of TPAs can also be explained in a different way. Fear et al. (2015) argued that large-scale TPAs should end up intersecting the cusp as their motion is controlled by the ionospheric/magnetospheric flow. Yet, another explanation has been proposed by Zhang et al. (2009) for a rare case where the entire polar cap is completely filled with auroral arcs. As this appears only during long-lasting strongly northward IMF, they suggested that dual lobe reconnection may be responsible for the nearly entire closure of open flux in the polar cap.

## 2.4 Plasma Sheet Thickening for Small-Scale Sun-Aligned Arcs

In Sect. 1.2, it was documented that small-scale Sun-aligned arcs and so-called horse-collar aurora are closely related geometrically. Specifically, the morning/evening web regions in Fig. 4a are filled with subvisible small-scale auroral arcs. One of the mechanisms for the formation of horse-collar aurora geometry is auroral oval expansion on the dusk and dawn sides during northward IMF conditions, which was first proposed by Meng (1981). Such poleward expansion of the oval corresponds to either the thickening or tilting of the central plasma sheet. These two models were later illustrated by Makita et al. (1991) as shown in Fig. 8b (plasma sheet tilting) and Fig. 8d (plasma sheet thickening). As shown in Fig. 8d, the central plasma sheet becomes thicker on the duskside which could lead to the poleward expansion of the oval as the evening web in the schematic illustration of horse-collar aurora by Hones et al. (1989) shown in Fig. 4a. The thickening of the plasma sheet may occur on the dawn and dusk sides simultaneously. In such a case, poleward expansion of the oval can happen on both sides and complete horse-collar aurora will appear.

## 2.5 Dayside Reconnection for TPA

Several studies in the 1990s proposed that a jump in the location of the reconnection site arising from an abrupt change in the IMF, either from northward to southward IMF or due

to a change in the  $B_y$  component, could somehow lead to the development of a new polar cap region equatorward of the old polar cap, causing a TPA to appear between the two regions of open field lines (Newell and Meng 1995; Newell et al. 1997; Chang et al. 1998). However, Fear and Milan (2012a) noted that the Chang et al. (1998) mechanism was incompatible with the fact that all points on the dayside magnetopause map to the open-closed field line boundary in the ionosphere. Furthermore, a correlation between an IMF  $B_z$  sign change and TPA formation could not be confirmed by observations (Kullen et al. 2002; Fear and Milan 2012a) except for the subgroup of TPAs called bending arcs (Kullen et al. 2002, 2015). For a description of bending arcs, see Sect. 1.1. The IMF conditions during which bending arcs occur deviate strongly from regular TPAs. As shown in Fig. 14a (red curve), most bending arcs form when IMF  $B_z$  is close to zero (or changes sign to weakly negative values). They appear at the dusk oval side for negative IMF  $B_y$  and at dawn for positive  $B_y$  (Kullen et al. 2002, 2015). Carter et al. (2015) proposed that the bending of the arc is probably caused by strong anti-sunward polar cap plasma flows in connection with dayside reconnection during  $|B_y| \gg |B_z|$  conditions (Fig. 14b and 14c). They suggest that bending arcs have, despite some apparent differences in shape, location, recurrence frequency and lifetime, a similar origin as poleward moving auroral forms (PMAFs). PMAFs are small polar cap arcs that split off the dayside oval and move poleward within a few minutes until they disappear (Fasel 1995; Milan et al. 2000), and are generally believed to be caused by flux transfer events (Frey 2007, and references therein). A detailed discussion of PMAFs can be found in Frey et al. (2019). In Kullen et al. (2015) several of Carter et al.'s (2015) ideas could be confirmed for a larger dataset. The connection to in situ FTE signatures, however, remains to be shown.

### 3 Recent Observations

#### 3.1 Arc Characteristics Seen in Ground-Based Optical Observations

Polar cap arcs have been routinely observed in ground-based all-sky imagers, for example imagers located at Longyearbyen, Svalbard ( $78.2^\circ$  N,  $15.7^\circ$  E), Ny-Ålesund, Svalbard ( $78.95^\circ$  N,  $11.9^\circ$  E), and Resolute Bay, Canada ( $74.7^\circ$  N,  $265.1^\circ$  E). The imagers are equipped with multiple optical filters and the most extensively utilized emissions for polar cap arc observations are at 557.7 and 630.0 nm wavelengths. The imagers have enabled comprehensive investigations of the motion of polar cap arcs. Hosokawa et al. (2011) carried out a statistical analysis using a large dataset by employing an automated algorithm for detecting polar cap arcs. They examined the motion of the Sun-aligned arcs on the duskside, midnight and dawnside separately. Figure 15 shows the distribution of the duskward velocity (on the vertical axis) of the duskside arcs (left), midnight arcs (middle) and dawnside arcs (right) as a function of the IMF clock-angle on the horizontal axis. The grey scale demonstrates the density of data points in percentage on a linear scale, self-normalized. Most of the arcs, especially those seen in the midnight sector, move in the direction of IMF  $B_y$ , which is consistent with the results of Valladares et al. (1994). However, many arcs move just poleward irrespective of the sign of IMF  $B_y$ . Such  $B_y$ -independent arcs are mostly seen either in the dusk side or dawn side. In particular, those seen on the dawnside have already been reported by a series of papers of Shiokawa et al. (1995, 1996, and 1997). They indicated that poleward moving Sun-aligned arcs are very common on the dawnside. The spatial structure is mostly Sun-aligned, but the temporal variations of these arcs are much more dynamic as compared to the  $B_y$ -dependent slowly moving arcs. The origin of this type of Sun-aligned

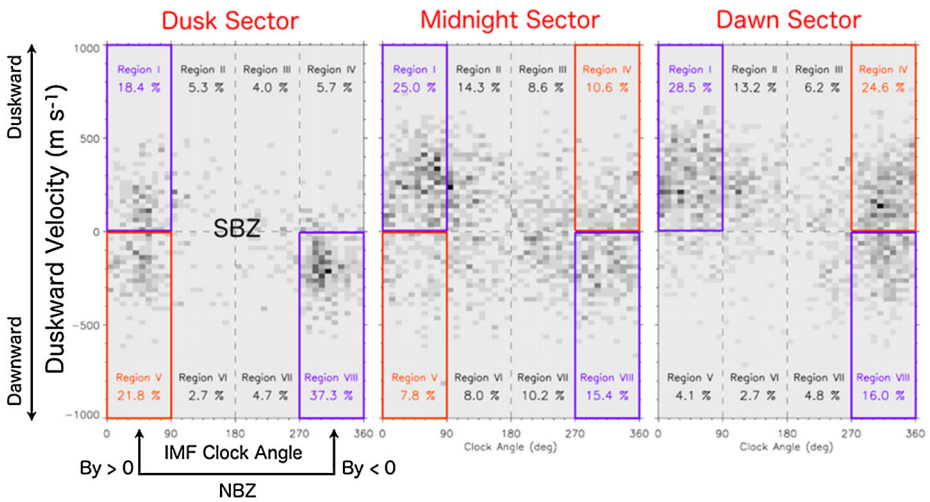


**Fig. 15** Statistical results on the dependence of the duskward velocity of polar cap arcs on the clock angle of IMF (taken from Hosokawa et al. 2011)

arc is still unknown, but Shiokawa and colleagues speculated, at that time, that these are associated with some boundary phenomena like Kelvin-Helmholtz instability, for example.

Most ground-based auroral observations of polar cap arcs are based on all-sky imager observations, as discussed above, but another type of observation can be made by examining auroral emissions on a very fine spatial scale. The Auroral Structure and Kinetics (ASK) instrument is a multi-spectral high-resolution imager located on Svalbard (Ashrafi 2007; Dahlgren et al. 2016). Due to its high-latitude location, ASK is perfectly situated for the study of polar cap aurora. ASK is capable of imaging auroral emission in three narrow (and separated) wavelength bands, in a field of view that corresponds to 55 km at 100 km altitude, and can resolve auroral structure down to spatial scales of tens of meters and temporal scales of tens of milliseconds. This capability has only been applied to a small number of events so far; the Reidy et al. (2017) multi-instrument study (discussed above) used ASK to conclude that a polar cap protrusion over Svalbard was consistent with formation on closed field lines. By comparing the ratio of two prompt emission wavelengths measured by ASK, they determined the energy of the precipitation causing the arc, which is usually only possible from space. The precipitation energy was found to be of the order of 5 keV, suggesting the electrons must have been accelerated. Coupled with the highly dynamic auroral structure seen by ASK, this observation demonstrates that this polar cap protrusion was occurring on closed field lines.

### 3.2 Small-Scale Electrodynamics in the Vicinity of Arcs

Measurements of small or meso-scale convection systems in the vicinity of polar cap arcs were carried out by using data from low-altitude satellite and incoherent scatter radars in 80's to early 90's (Burke et al. 1982; Frank et al. 1986; Robinson et al. 1987; Carlson et al. 1988; Valladares and Carlson 1991). One consensus from these series of measurements is that polar cap arcs are always associated with strong shear in the background convection (i.e.,  $\mathbf{E} \times \mathbf{B}$  drift), which corresponds to the electric field structure converging towards the arc. Such converging electric field structure can drive horizontal Pedersen currents also flowing towards the arc which are closed by the upward field-aligned currents within the arcs.

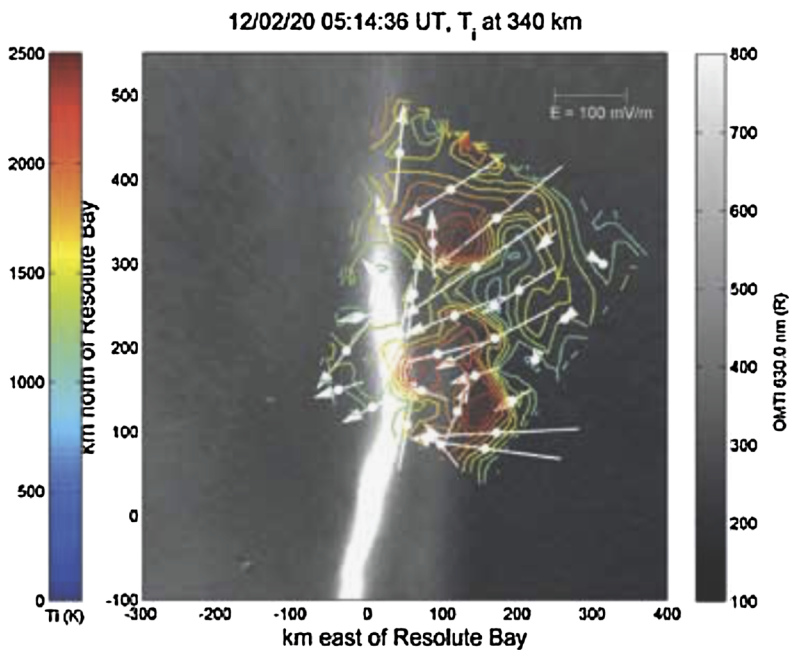


**Fig. 16** Simultaneous radar and optical observations of a polar cap arc at Resolute Bay, Canada (taken from Dahlgren et al. 2014)

In these earlier studies, however, due to the limitation in the temporal resolution of the radar measurements, it was difficult to visualize the convection pattern in a two-dimensional fashion. Recent simultaneous ground-based imager and radar (both coherent and incoherent scatter) measurements have been of great value in revealing the electrodynamics of polar cap arcs. Especially, in the last decade, a phased-array incoherent scatter radar at Resolute Bay, Canada has been used for observing 3D electrodynamics in the vicinity of polar cap arcs in combination with all-sky imagers situated in the same place. In addition, several coherent high-frequency (HF) radars of SuperDARN were deployed in the polar cap latitudes which can be used for simultaneous observations of Sun-aligned arcs with all-sky imagers.

Koustov et al. (2008, 2012) found that in comparison to the background polar cap, polar cap arcs are associated with decreased and increased power of radar echoes coming back from the E- and F-regions, respectively. The spectrum of these echoes is broadened. Plasma flow is enhanced on the dawn- and duskside of the arc and across the arc the flow exhibits a sharp reversal from sunward to anti-sunward direction. Since the plasma motion is governed by the local  $\mathbf{E} \times \mathbf{B}$ -drift, the radar's measurements of plasma flow represent the distribution of converging electric fields in the vicinity of the arc. Figure 16 shows one of the other examples from simultaneous radio and optical observations of a Sun-aligned arc by the incoherent scatter radar and all-sky imager at Resolute Bay (Dahlgren et al. 2014). They observed strong electric field directed towards the arc, which is consistent with the converging electric field reported in the earlier studies. They also indicated that the ion temperature was significantly enhanced in the region adjacent to the arc through the Joule heating effect of the electric field; thus, the magnitude of the flow (and corresponding electric field) was large only in a localized region near the arc.

By examining the similar incoherent scatter radar's electron density measurements, Perry et al. (2015) noted that the leading edge of the arc is associated with a meridionally extended plasma density depletion in the F-region ionosphere, located partially within a downward field-aligned current region. Samara and Michell (2013) found that the altitude profile of the ionization produced by polar cap arcs is consistent with that expected for precipitating electrons accelerated by Alfvén waves. Kozlovsky et al. (2007) studied morning-side arcs and found that each arc was associated with four specific FAC regions: the upward FAC region containing the optical arc, the return downward FAC region poleward of the arc; and a secondary weaker arc equatorward of the main arc with a pair of FACs similar to the main arc. Zhang et al. (1999) identified a strong horizontal electrojet flowing along the arcs as carried by the electric field drift of the low-energy electrons within the arc.

### 3.3 Optical and in-Situ Particle Signatures at Low-Altitude

Over the last 15 years, four SSUSI instruments have been deployed on DMSP spacecraft F16-F19 (Paxton et al. 2002). When over the polar regions, the SSUSI instruments scan anti-sunward along their orbit, building up an image of a swath of the auroral region over 20 minutes. These instruments provide an excellent opportunity for near-simultaneous, inter-hemispheric observation of polar cap arcs. The DMSP satellites have also carried sensors to measure auroral precipitation since 1973 (Hardy 1984). Hardy et al. (1982) found examples of polar cap arcs embedded within polar rain, suggesting to them that the source region of these arcs was likely to be on open field lines. More recently, a renewed interest in these in-situ measurements have been reported, particularly since the SSUSI instruments were placed on DMSP satellites.

Reidy et al. (2017) combined SSUSI images with multiple other instruments, to demonstrate that polar cap arcs occurring on both open and closed field lines could occur simultaneously. The SSUSI observations showed a feature protruding into the duskside of the polar cap in both hemispheres, which lasted several hours. This feature was termed a 'failed trans-polar arc' as it did not cross the entire polar cap but was consistent with a closed field line formation mechanism. The arc 'failed' due to a southward turning of the IMF. A clear Sun-aligned arc stretching across the polar cap was observed on the dawnside of the northern hemisphere in the same SSUSI image. This arc was consistent with formation on open field lines (see also Sect. 1.3 and 5.2). Carter et al. (2017) and Xing et al. (2018) presented separate SSUSI observations of polar cap arcs occurring simultaneously in both hemispheres that were found to be consistent with formation on closed field lines. In the case of Carter et al. (2017), they showed two transpolar arcs occurring in both hemispheres simultaneously. This observation demonstrated the complex configuration of the Earth's magnetotail during northward IMF, such that two 'tongues' of closed flux could co-exist in the otherwise open polar cap. By surveying one month of SSUSI images with the corresponding particle data, Reidy et al. (2018) found examples of polar cap arcs consistent with open and closed field lines. These studies demonstrate that low-altitude UV imagers can provide near-simultaneous measurements of both hemispheres and are capable measuring polar cap arcs occurring on both closed and open field lines.

Low altitude in-situ particle data, such as that from DMSP, provide an excellent insight into the topology of the polar cap. Newell et al. (2009) used these data to suggest that there are three different formation mechanisms for polar cap arcs: two which occur on closed fields and one on open. Fear et al. (2014), Carter et al. (2017) and Xing et al. (2018) presented DMSP particle observations, as well as observations from multiple ground-based and spacecraft instruments, of transpolar arcs occurring on closed field lines. The DMSP particle detector measured ion and electron precipitation associated with each of these arcs. The

DMSP data presented by Fear et al. (2014) also showed electron-only signatures on either side of the transpolar arc that did not correspond to arcs observed by the IMAGE FUV imager, suggesting the possible simultaneous presence of open field line polar cap arcs, as subsequently shown by Reidy et al. (2017). Cumnock et al. (2009) used DMSP particle data to examine the structure within large scale PCAs, finding a small number of them to be composed of multiple distinct thin arcs, each associated with ion precipitation. Additionally, Reidy et al. (2017) presented an observation of a Sun-aligned arc seen in the SSUSI images that was associated with electron-only precipitation in the corresponding DMSP particle data. This arc was found to be consistent with open field lines formed by accelerated polar rain. Also discussed above, the Reidy et al. (2018) survey found examples of arcs occurring on both open and closed field lines using corresponding auroral and particle data from DMSP satellites. These studies demonstrate the importance of in-situ particle data and show that these low-altitude observations provide information about the topology of the polar cap that is not evident from images alone.

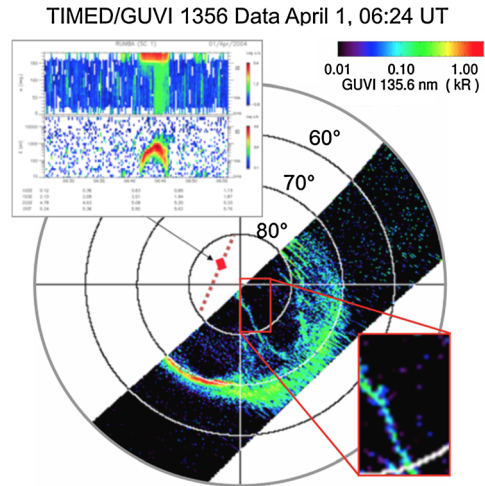
### 3.4 Fine-Scale Particle Characteristics at High-Altitude

In the 1990s the Polar spacecraft and the ISEE (International Sun-Earth Explorer) spacecraft provided the first in-situ observations at high-altitude above polar cap arcs. These high-altitude observations were used to investigate the magnetic field line topology of polar cap arcs and the magnetospheric region to which they are connected (see Zhu et al. 1997 and references therein). Since their launch in 2000 into a polar orbit, the 4 Cluster satellites have sampled the lobe region above the polar caps at high altitude, providing new insight on the configuration of the high latitude magnetosphere during periods of low geomagnetic activity. They revealed the presence of upflowing ionospheric ion beams with typical inverted-V structures in time-energy spectrograms above the polar cap during periods of low geomagnetic activity typically at altitudes between  $\sim 5 R_E$  and  $\sim 9 R_E$  (Maggiolo et al. 2006). These polar cap ion beams (PCIBs) are accelerated by quasi-static electric field structures located above the polar ionosphere during periods of northward IMF. In a latter statistical study, Maggiolo et al. (2011) showed that PCIBs display similar properties as small-scale Sun-aligned arcs, like their dependency on IMF or their width and orientation in the Sun-Earth direction. Later the association between PCIBs and small-scale Sun-aligned arcs was definitely proven during a conjunction between Cluster and TIMED (Thermosphere Ionosphere Mesosphere Energetics Dynamics) satellites (see Fig. 17 taken from Maggiolo et al. (2012) for detail).

Contrary to low altitude observations (see Sect. 3.3) which are restricted to the observation of precipitating particles, high altitude observations sample the particle and fields inside or above the acceleration region. PCIBs are generated by quasi-static electric field structures which accelerate ions upward and electron downward, triggering the optical emission of the associated polar cap arcs. Interestingly, Cluster observations at high altitude reveals that the electric field parallel to the magnetic field extends to higher altitudes above the polar caps (up to  $\sim 5 R_E$ ) compared to similar structures in the auroral zone. Furthermore, the total field aligned potential drop in the polar cap region is typically of a few hundreds of Volts, one order of magnitude lower than the potential drop associated with inverted-Vs in the auroral zone. As discussed in Sect. 1.3, particle observations at high altitude by the Cluster spacecraft revealed that PCIBs are associated with the precipitation of polar rain-like electrons and often with the simultaneous presence of plasma sheet like electrons which leads to questions about the magnetic field line topology.

In-situ observations at high altitude benefit from the low spacecraft velocity and the large spatial extension of the magnetic flux tubes connected to polar cap arcs. This allows a much

**Fig. 17** Image of the northern polar cap from the GUVI experiment onboard the TIMED spacecraft. The red dotted line shows the projected orbit of the Cluster spacecraft and the red square the projected location of the inverted-V detected by Cluster. Bottom right: detail of the polar cap arc detected by GUVI. Top left: Cluster HIA observation of the ion inverted-V associated with the polar cap. Top: ion pitch angle distribution from HIA for all ions. Bottom: time-energy spectrogram from HIA for all ions. See Maggiolo et al. (2012) for more details



better sampling of the particles and fields. For instance, the return current region associated with PCIBs and thin Sun-aligned polar cap arcs, whose width is only of a few km at ionospheric altitude, has been clearly identified with the Cluster spacecraft (Teste et al. 2007). Carried by upflowing low-energy electrons accelerated by a quasi-static electric field (typically  $\sim 50$  V), the return current has the same intensity as the upward current inside which points to a local closure of the current system. High-altitude observations thus have significant advantages. However, as they are made far from the ionospheric level where polar cap arc emissions occur, it is not always obvious to make a one-to-one correspondence between them and polar cap arcs. That is why they clearly benefit from conjugate observations made either by imagers or low-altitude spacecraft.

### 3.5 Relationship with Large-Scale Convection

The large-scale convection pattern can be observed with the SuperDARN (Chisham et al. 2007). Studies have been undertaken which determine the general morphology of convection during periods of northwards IMF, and there are studies which focus specifically on convection at times when TPAs are present: for instance, Milan et al. (2005), presented in Fig. 9, and Goudarzi et al. (2008), presented in Fig. 18. During northward IMF conditions, three main features are observed: (1) a cessation of the typical twin-cell convection pattern associated with the Dungey cycle during periods of southwards IMF, (2) sporadic but weak bursts of nightside reconnection which lead to enhanced nightside convection, often with a significant eastward or westward component to the flow, known as TRINNIs (see Sect. 2.2), (3) lobe reconnection at the magnetopause which leads to sunwards convection and the formation of reverse lobe cells in the noon sector polar cap. Features (1) and (3) are well-known from early studies of the average morphology of convection for different orientations of the IMF (e.g. Ruohoniemi and Greenwald 1996). Feature (2), first studied in-depth by Grocott et al. (2003, 2004), was less-well understood due to the sporadic nature of the flows; moreover, as TRINNIs do not have a significant auroral or geomagnetic signature associated with them (Milan et al. 2005), they were not discovered until regular measurements of convection were available.

It is found that the convection during TPA events is no different from the general northward IMF morphology, but that TPA formation and motion can be understood in terms of this

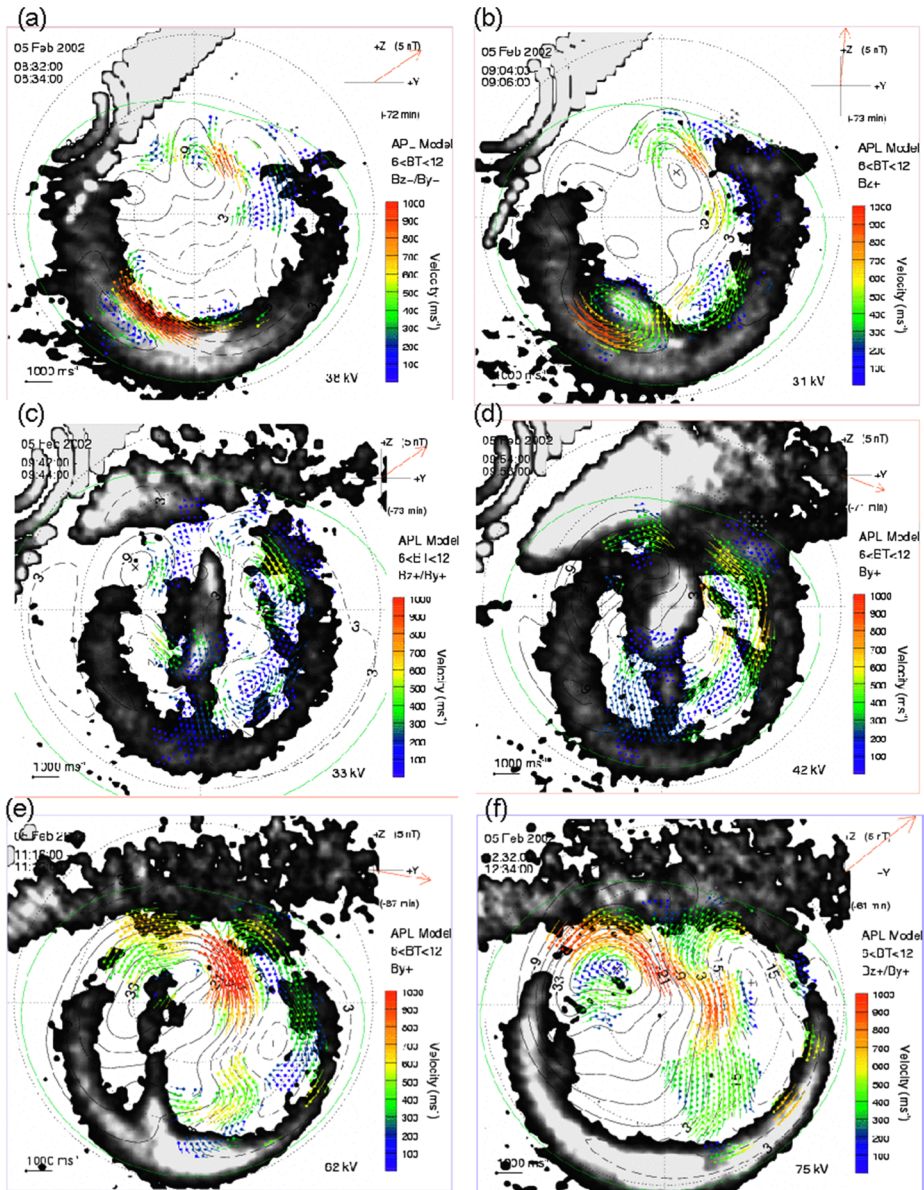


**Fig. 18** A sequence Far Ultraviolet Wideband Imaging Camera (FUV-WIC) images from 5 Feb 2002, with superimposed SuperDARN convection maps. (From Goudarzi et al. 2008)

morphology. Specifically, under certain circumstances, which are presently not understood, the occurrence of a TRINNI can lead to the protrusion of a tongue of closed magnetic flux into the otherwise open polar cap (see Sect. 2.2), with the TPA being associated with plasma sheet-like precipitation on these closed field lines (Milan et al. 2005; Fear and Milan 2012b; Fear et al. 2014). Once formed, the closed field lines which constitute the TPA are entrained within the general polar cap convection of the surrounding open field lines, what-



ever the source of that convection may be. For instance, “lobe stirring” produced by lobe reconnection can cause dawnward and duskward motion of the TPA (Milan et al. 2005; Carter et al. 2017); twin-cell convection associated with southwards IMF can cause the TPA to be pushed towards the nightside (Milan et al. 2005; Reidy et al. 2017); or twin-cell convection with a significant east-west asymmetry associated with IMF  $B_y$  can lead to dawnward or duskward motions (Goudarzi et al. 2008).

### 3.6 Interhemispheric Symmetry/Asymmetry

So far there have only been two opportunities for true simultaneous optical observations of polar cap aurora from space, by the DE-1 and Viking satellites in the 1980s (Craven et al. 1991), and by Polar and IMAGE in the 2000s (Østgaard et al. 2003). As discussed in Sect. 1.1., earlier particle measurements in both hemispheres hinted at some conjugacy between transpolar arcs and a similar but opposite motion towards dawn/dusk depending on the sign of the IMF  $B_y$  component. This symmetry was used as an argument for magnetic mapping from a single magnetospheric source, and thus the occurrence of transpolar arcs on closed field lines (Craven et al. 1991). But true interhemispheric observations and the determination of the degree of conjugacy was only possible with space-based imagers.

During a period in 1986 simultaneous images by Viking in the sunlit northern hemisphere and by DE-1 in the dark southern hemisphere revealed the simultaneous presence of transpolar arcs in both hemispheres (Craven et al. 1991). Mapping of the arcs between the hemispheres showed that they were slightly rotated with respect to the noon-midnight meridian and that they were slightly offset in the dawn-dusk direction. These measurements also confirmed their occurrence during northward IMF and a dawnward motion in the northern hemisphere during positive  $B_y$  and an opposite motion in the southern hemisphere. Overall there has been only a 20-minute overlap of the observations and a number of open questions remained unanswered like topological variations of the magnetotail in response to changes in the IMF orientation and the related direction of motion of the arcs.

The ultraviolet cameras on IMAGE and Polar provided a new opportunity for interhemispheric aurora observations. In two cases a transpolar arc could only be observed in one hemisphere, but not the other. These two cases were discussed in 3 different papers (Østgaard et al. 2003, 2007; Frey 2007). In one particular case (see Fig. 19) also several passes by DMSP satellites allowed for the measurement of precipitating electrons and ions and plasma drift. The northern hemisphere images showed a clear transpolar arc with an intensity similar to the brightness of the auroral oval. In the southern hemisphere however, there was no sign of any aurora inside the polar cap. The particle measurements in the northern hemisphere show that the arc was produced by 0.4–1 keV electrons while simultaneous 1–10 keV ions indicated that the arc was on closed field lines with surrounding open field line regions on both sides (Fig. 19d). Contrary, in the southern hemisphere no indication of any energetic precipitation could be detected but rather polar rain features that are signatures of open field lines. Plasma drift measurements in the northern hemisphere showed two narrow regions of sunward flows adjacent to an anti-sunward flow at the location of the transpolar arc. The additional presence of a bright proton aurora cusp spot (Frey et al. 2019) further supported the overall picture of a 4-cell convection pattern during northward IMF with the arc located between the cells (Newell et al. 2009). A similar convection pattern was observed in the southern hemisphere but as it was not related to any visible aurora or particle precipitation it appeared that the theta aurora was a non-conjugate phenomenon (Østgaard et al. 2003).

The authors discussed several reasons for the absence of theta aurora in one hemisphere, including conductivity differences in the sunlit and dark ionospheres (Shue et al. 2001;

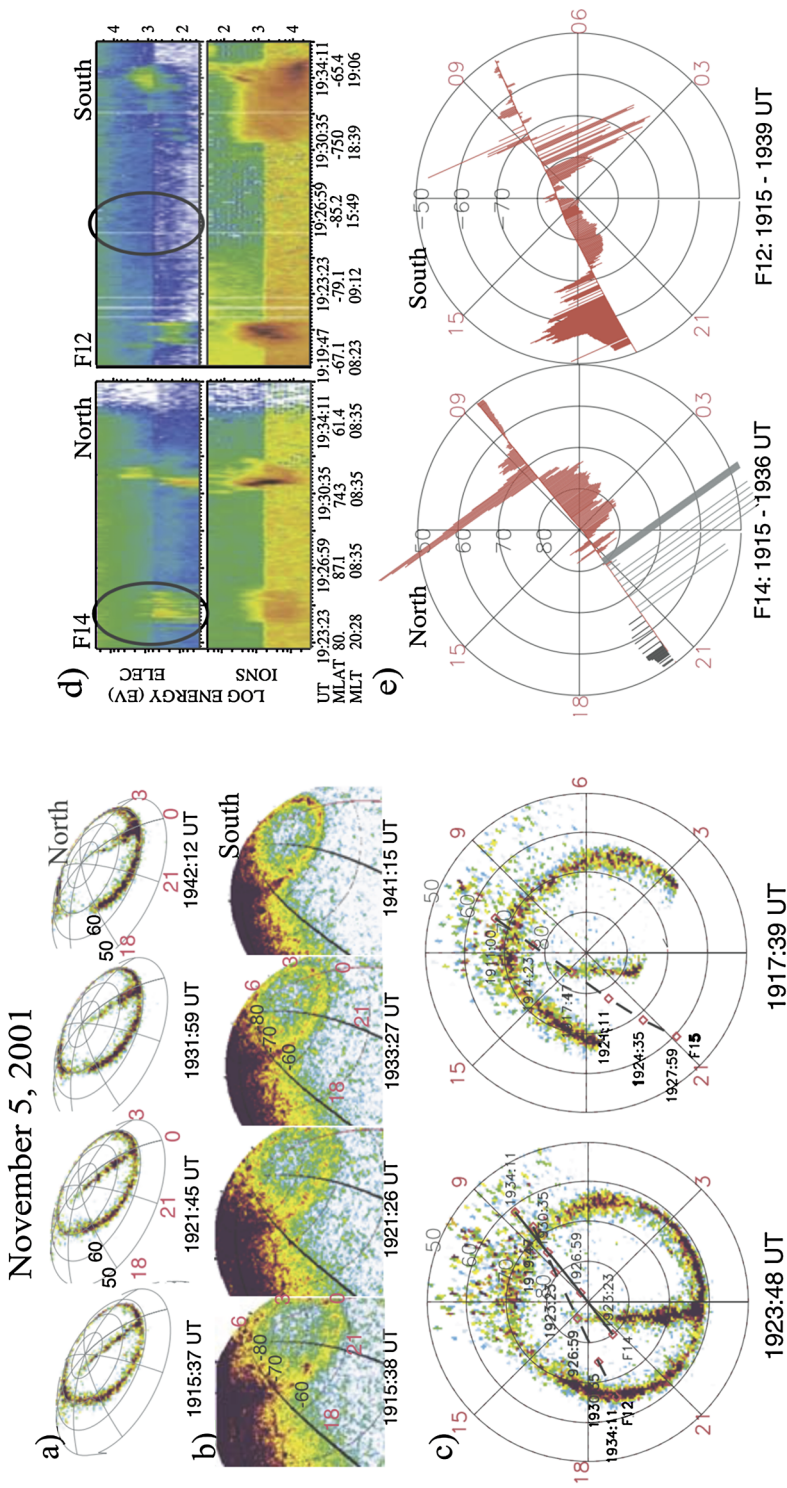


**Fig. 19** Interhemispheric observations of a non-conjugate transpolar arc on November 5, 2001 (from Østgaard et al. 2003). **(a)** The IMAGE SII3 observed the northern hemisphere (NH). **(b)** The Polar VIS Earth camera observed the southern hemisphere (SH). **(c)** Trajectories of nearly simultaneous DMSP passes (solid; NH, dashed; SH) mapped onto simultaneous SII3 images from the NH. **(d)** Spectrograms from DMSP, electrons and ions, where the ovals signify the expected location of the theta auroral precipitation (if any). **(e)** Cross track plasma drift data from DMSP. Grey color indicate data where the amplitude is not correct

Wiltberger et al. 2009) and the dipole tilt angle (Kullen 2012). In the end they found it most reasonable that the IMF  $B_x$  component determines in which hemisphere lobe reconnection is most efficient, in the northern hemisphere for negative  $B_x$  and in the southern hemisphere for positive  $B_x$  (Stubbs et al. 2005; Laundal et al. 2018). This is in agreement with statistical studies about the  $B_x$  effect on high-latitude aurora (see Chap. 1.4 for references). The resulting 4-cell convection pattern can then drive flow shears with sufficient strength to generate strong electric fields just in one hemisphere which then accelerate electrons to create aurora (Østgaard et al. 2003, 2005, 2007).

The interhemispheric observational results can now also be modeled with magnetohydrodynamic simulations (Watanabe and Hairston 2016). A specific field-aligned current system is set up in connection to the formation of drifting theta aurora in response to the  $B_y$  direction during northward IMF. When the IMF  $B_y$  changes from positive to negative a transpolar arc in the northern hemisphere moves downward. In the southern hemisphere the arc moves into the opposite direction. The polarity of the field-aligned current system reverses accordingly.

The combination of IMAGE in the southern hemisphere and one of the DMSP satellites in the northern hemisphere allowed for some study of the dynamics of transpolar arcs in both hemispheres (Carter et al. 2017). The dawnside arc in the northern hemisphere traversed to the duskside responding to a negative to positive change of the IMF  $B_y$ . At the same time, the duskside arc in the southern hemisphere traversed the polar cap to the dawnside. As the arcs are connected to closed field lines a complex magnetic field line topology must develop protruding into the otherwise open polar cap. These observations supported the hypothesis that transpolar arcs form on closed field lines and are entrained within the ionospheric convection. The IMAGE/Polar combination of interhemispheric observations was also used to determine asymmetries in the polar cap boundary location (Laundal et al. 2010). It was shown that the northern and southern auroral ovals encircle the same amount of magnetic flux and that the aurora poleward boundaries thus mark the open/closed field line boundary. Rapid magnetic flux closure in the magnetotail however can lead to strong asymmetries between the hemispheres as a response to differences in the ionospheric convection. The different amount of solar illumination is the most logical reason for the differences in convection.

### 3.7 Ionospheric Scintillation Associated with Polar Cap Arcs

Data from ground-based imagers, which are introduced in 3.1, have been compared with Global Navigation Satellite Systems (GNSS) to study how polar cap arcs ionize and structure the ionospheric plasma and affect the performance of the Global Positioning System (GPS) in the polar regions. Jayachandran et al. (2009, 2012) found that the ionospheric total electron content (TEC) can vary by  $\sim 3$  TEC units during the transit of the arc, the amplitude of the variation decreasing as arcs move poleward from the source regions. Jayachandran et al. (2017) detected amplitude and phase scintillations, which are rapid random fluctuations of the amplitude and phase of trans-ionospheric radio signals, in close association with polar cap arcs, indicating the occurrence of kilometer scale electron density fluctuations, i.e., irregularities, in the ionosphere. On the other hand, van der Meeren et al. (2016) used DMSP SSUSI images to study the presence of irregularities in the ionosphere and scintillation caused by polar cap arcs. They used multiple other data sources and concluded, in this case, that the polar cap arc was only a weak source of irregularity.

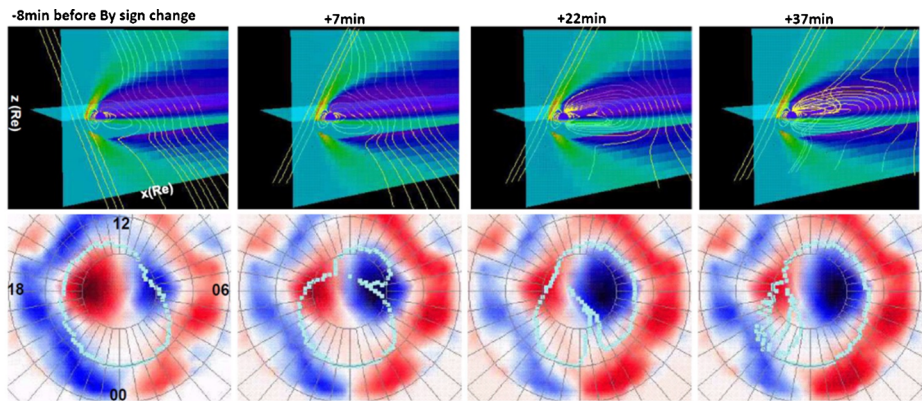


**Fig. 20** MHD simulations of an IMF  $B_y$  sign reversal during northward IMF by Kullen and Janhunen (2004). The top row shows IMF and tail B-field in a 3-D view of all B-field lines crossing the  $x$ -axis. The bottom row shows the northern hemisphere in a polar view with the sun at the top. The blue and red colors mark the current densities, overlaid in light blue is the open-closed field line boundary

## 4 Recent Modeling Results

### 4.1 MHD Simulation for $B_y$ -Switching

As discussed in Sect. 1.4, a TPA that moves over the entire polar cap from one oval side to the other, appears typically in connection with an IMF  $B_y$  sign change during predominantly northward IMF conditions (e.g., Cumnock 2005). Simulating such IMF conditions with an MHD model results in conjugate TPAs that move in each hemisphere in opposite directions over the model polar cap, as expected from observations. This is shown in Fig. 20, containing a 3-D view of IMF and magnetosphere B-field lines from a simulation by Kullen and Janhunen (2004) in the first row, and a polar view on the northern hemisphere in the second row. Four points of time are shown before and after the sign change has reached the dayside magnetopause. The plots show that the open-closed field line boundary in the model ionosphere (light-blue curve in bottom plot) becomes bifurcated after the  $B_y$  sign change, and that this finger of closed field lines (which is assumed to be the location of a TPA) propagates over the entire polar cap while the tail B-field undergoes a major tail reconfiguration.

The good agreement between IMF  $B_y$  sign-change simulation results of several different MHD codes allows us to draw conclusions about the connection between TPA motion and changes in the magnetotail topology. Slinker et al. (2001) used for their simulations the Fedder and Lyons model, Kullen and Janhunen (2004) the GUMICS-3 code, Naehr and Tof-foletto (2004) the BATSRUS model, and Tanaka et al. (2004) an earlier version of REPPU code. The results from the different MHD codes are compared in Fig. 21. It contains ionospheric and magnetotail plots from these four different MHD codes about 20–30 minutes after an IMF  $B_y$  sign change reached the dayside magnetopause. The top row shows the open-closed field line boundary in the northern ionosphere, the bottom row the plasma pressure distribution (in the right plot only the open-closed field line boundary) at tail cross sections in the mid tail. In each MHD simulation the plasma sheet (closed field line region in right plot) has become strongly kinked (bifurcated). The bifurcated plasma sheet part maps to a finger of closed field lines that stretches into the polar cap (the assumed location of a TPA), as is easily seen in the middle plots where the black squares along the TPA are mapped back to the plasma sheet in the tail cross section. Note, also Maynard et al. (2003)

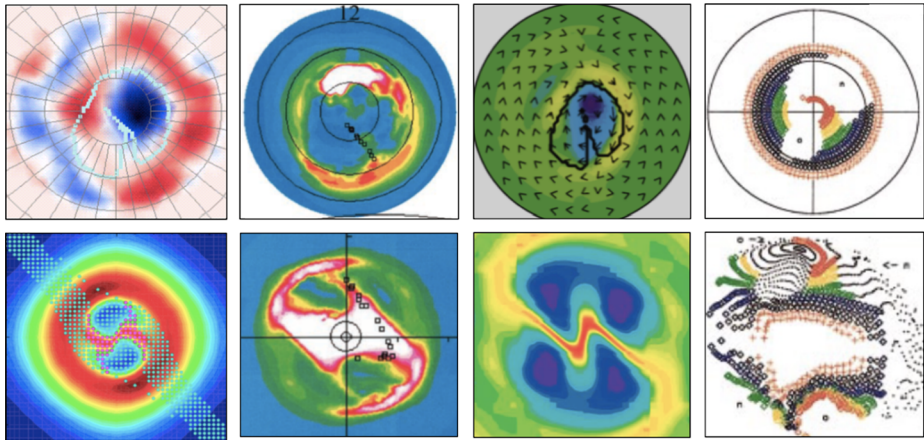


**Fig. 21** MHD simulations of a  $B_y$  sign reversal during northward IMF by Kullen and Janhunen (2004) (left), Tanaka et al. (2004) (middle left), Naehr and Toffoletto (2004) (middle right), and Slinker et al. (2001) (right column) 20 min, 24 min, 26 min, and 30 min after the sign reversal. The top row shows the open-closed field line boundary in the northern ionosphere (polar view with Sun at the top) (from left to right) as a blue curve, black squares, and a black curve. The background colors mark current density (left and right plots) and plasma pressure isocontours (middle plot). The bottom row shows the tail cross section at (from left to right)  $x = -30 R_E$ ,  $-15 R_E$ , and  $-24 R_E$  with color coded plasma pressure isocontour lines. In the left plot the open (blue dots) and closed (pink dots) field lines are overlaid over the plasma pressure, in the right plot only the closed field line region is shown (plasma pressure plots not shown in Slinker et al. 2001)

studied a  $B_y$  sign change run (not shown here), however in the IRM model they used, only small bulges appeared at the open closed field line boundary, which the authors assumed to represent small-scale arcs.

How such a deformed plasma sheet shape evolves after an IMF  $B_y$  sign change, is examined in detail in Kullen and Janhunen (2004) and in Naehr and Toffoletto (2004). The results have been summarized in the schematic of Fig. 9b. As mentioned already in Sect. 2.1., the original (IMF  $B_y$  induced) plasma sheet twist does not change immediately in the entire tail after a sign reversal. The plasma sheet flanks and the near-Earth tail are affected first. Thus, in an intermediate state, the plasma sheet in near-Earth and far tail are oppositely twisted. Looking at a tail cross section in the mid tail, the flanks' parts are already twisted in the new direction while the central part keeps its old twist, resulting in the strongly kinked (bifurcated) shape, shown in Fig. 21 for the different models. As time passes, the bifurcated part propagates through the lobe from one flank to the other. It maps to the closed field line strip (TPA) that moves over the entire polar cap, until the entire tail is twisted in the opposite direction and the model TPA disappears.

Studying the reconfiguration of the tail lobes during the sign change shows that a new region of open field lines appears (for a sign change from dusk- to dawnward) in the northern hemisphere at the dusk flank (marked in orange in the schematic of Fig. 9b) which expands at the expense of the old open flux region at the dusk lobe (marked in red). In the southern lobe, new and old regions appear on the opposite sides. The formation of the new lobe can be understood by considering the redistribution of open field lines through high-latitude lobe reconnection during northward IMF. In general, old lobe field lines are transformed through reconnection with IMF field lines into new open field lines that are first draped over the dayside magnetopause until they eventually move along the flanks tailward. For dusk-northward IMF, a (at the high-latitude lobe reconnected) newly oriented open field line will

have the same dawn-dusk tilt as the surrounding IMF, and thus propagates from the dayside magnetopause towards the dawnside flank and further tailward (e.g., Fig. 1 in Crooker and Rich 1993). After an IMF  $B_y$  sign change, a new (in the northern hemisphere created) open field lines will no longer move along the dawn flank but along the dusk flank to the tail (as is expected for the new, downward  $B_y$  direction). Thus, the duskside grows at the expense of the dawnside part of the northern lobe.

The different MHD studies could clarify several other IMF effects on TPAs as well. An IMF  $B_y$  sign change during southward IMF does not cause a TPA (Maynard et al. 2003), which is in agreement with observations. This is probably due to the smaller plasma sheet twist and a shorter tail (i.e. shorter region of closed tail field lines) during southward IMF (Kullen and Janhunen 2004). Slinker et al. (2001) showed by comparing observations with simulations that an IMF  $B_y$  sign change during weak and strong northward IMF results in both cases in a TPA that moves over the entire polar cap, but in the latter case the polar cap is considerably contracted. Their results demonstrate that this is connected to a considerable thickening off the plasmas sheet, especially at its flanks (see also Sect. 4.2 about MHD simulations of the horse collar oval). Naehr and Toffoletto (2004) simulated two  $B_y$  sign changes separated by one hour, resulting in the formation of a second TPA at the opposite oval side. Their results showed that the first TPA did not disappear but moved slightly back to the oval side it came from, thus offering a possible explanation for the often observed simultaneous existence of two TPAs on opposite oval sides (see Sect. 1.1 and Fig. 1).

There are a number of qualitative differences between observations and the simulation results, such as a too short and thick TPA, too short TPA lifetime, a too short tail etc. However, these discrepancies may disappear with better resolution in the model tail and more advanced modeling of the ionosphere (see, e.g. the promising mapping results from Tanaka et al. 2017 presented in Sect. 4.2). A more fundamental question is, whether a plasma sheet filament (that stretches into the lobes and maps to a TPA) can form without local tail reconnection or not. According to Milan et al.'s (2005) conceptual TPA model, such reconnection is required (see Sect. 2.2). On the other hand, Tanaka et al.'s (2004) detailed examination of the magnetic field line convection after the  $B_y$  sign change revealed, that a return flow blockage in the convection cells after an IMF  $B_y$  sign change may be responsible for the pileup of closed flux at the location of the bifurcated plasma sheet. Whether this pile-up of closed flux is created by reconnection or is just a result of redistributing field lines is not addressed by Tanaka et al. (2004) and remains to be shown (note that, just recently, a newer version of REPPU code was applied to the theta aurora case and the results are introduced in Tanaka et al. 2018).

Further investigations (both simulation-based and observational) should be performed to examine this matter in more detail. Note also, that all TPA simulations discussed in this section require an IMF sign change for a TPA to appear and move over the polar cap. As discussed earlier (in Sect. 1.4) a sign change is not an observational necessity for a TPA to occur (e.g., Fear and Milan 2012a). This is indicated in more recent MHD simulation runs for northward IMF with a constant IMF  $B_y$  component as well. In Maynard et al.'s (2012) simulations a plasma sheet bifurcation occurs close to the flanks, in Tanaka et al.'s (2017) simulations polar cap arcs occur close to the dawn and dusk oval. The results of the latter model are discussed in more detail in the next section.

## 4.2 MHD Simulation of Sun-Aligned Arcs

As introduced in Sect. 4.1, several global MHD simulations have been carried out to understand the formation process of large-scale transpolar arcs. In contrast, it has been difficult to

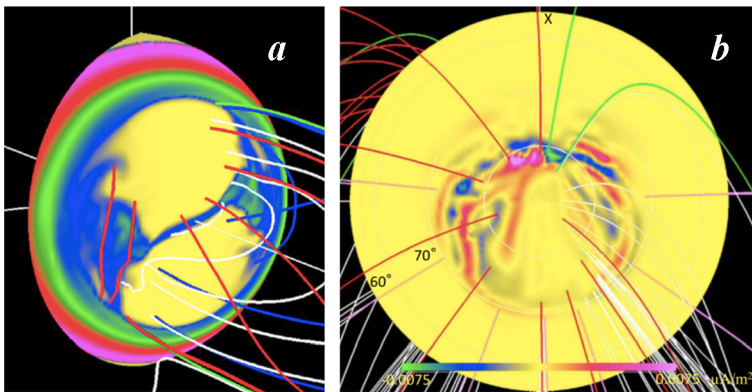


**Fig. 22** (a) Cross section of pressure distribution (colors), last closed magnetic field lines, and the nightside separator. The radial distance of the cross section is  $22 R_E$ . (b) Equivalent ionospheric projection of the FAC and magnetic field lines. The size of the sphere is  $3 R_E$ . This figure is looked down from just over the North Pole. The FAC is shown by colors (– upward, + downward). The  $60^\circ$ ,  $70^\circ$ , and  $80^\circ$  northern latitudes are back projected from the ionosphere along the dipole field (taken from Tanaka et al. 2017)

reproduce small-scale Sun-aligned arcs or horse-collar aurora in MHD simulations because of insufficient spatial resolution. Recently, Tanaka et al. (2017) reproduced signatures of small-scale Sun-aligned arcs on both the dawn and dusk sides of the polar cap (i.e., horse-collar aurora) by improving the mesh resolution in the ionospheric side of the simulation. Figure 22a shows a cut of the tail and the blue structure in the pressure is the plasma sheet. Tanaka and colleagues did not consider any big changes in the IMF  $B_y$ . However, significant thickening of the plasma sheet is seen on the duskside and dawnside. Figure 22b is the field-aligned current distribution in the ionosphere, and the horse collar structure is clearly reproduced as a bundle of small-scale Sun-aligned arcs. Tanaka et al. (2017) noted that the origin of the shear flow producing FAC in the region of Sun-aligned arcs is still unclear, but at least they demonstrated that Sun-aligned arcs in the horse collar aurora system are caused by this kind of thickening of the plasma sheet on closed field lines.

## 5 Unclarified Issues

### 5.1 Origin of the Dawn-Dusk Motion of Arcs

As introduced in 1.4, the dawn-dusk motion of large-scale TPA is known to be controlled to a large extent by the  $B_y$  component of the IMF (e.g., Frank et al. 1986; Rairden and Mende 1989; Kullen et al. 2002; Milan et al. 2005; Carter et al. 2017). Not only large-scale arcs, but also small-scale Sun-aligned arcs in the polar cap region are known to move in the dawn or dusk direction depending on the sign of the upstream IMF  $B_y$ , as for example demonstrated by Hosokawa et al. (2011) and introduced in 3.1. These studies indicated that in the northern hemisphere polar cap arcs move in the direction of IMF  $B_y$ . That is, when the IMF  $B_y$  is positive arcs move duskward while they move dawnward when the IMF  $B_y$  is negative. The speed of the arcs ranges from 50 to 150 m/s in the dawn-dusk direction.

The entrainment of the TPA within the convection pattern is exemplified by the examples reported by Milan et al. (2005) and Goudarzi et al. (2008), shown in Figs. 10 and 18, respectively. In Fig. 10, both before and after the TPA has formed, flows in the noon sector

polar cap suggest the presence of reverse lobe cells associated with lobe reconnection (left and middle panels). In the middle panel, the prenoon lobe cell is focused on the sunward tip of the TPA, and the redistribution of open/closed flux within the polar cap associated with this convection is thought to give rise to the dawn-dusk motion of the TPA (middle and right panels). Furthermore, following a southward turning of the IMF, the development of typical Dungey cycle twin-cell convection flow is observed (right panel), and the addition of new open flux to the dayside polar cap by low latitude reconnection increases the size of the polar cap (seen as an equatorward expansion of the auroral oval) and pushes the TPA towards the nightside. The control of the motion of TPA, in particular in the dawn-dusk motion, by the  $B_y$  and  $B_z$  components of IMF is schematically depicted in Fig. 8 of Milan et al. (2005). This model can also explain the  $B_y$ -controlled motion of small-scale Sun-aligned arcs (Hosokawa et al. 2011). In Fig. 18 the sequence of images shows that following the formation of the TPA, a southward turning of the IMF with significant  $B_y > 0$  leads to twin-cell convection with most convection flow into the dawn-sector polar cap, causing a duskward motion of the TPA (panels (e) and (f)).

## 5.2 Open/Closed Issue

Conflicting conclusions on whether polar cap arcs occur on open field lines (e.g. Hardy et al. 1982) or closed field lines (e.g. Frank et al. 1982) have been proposed since the 1980s. Despite a number of studies dedicated to this issue, the magnetic field line configuration is still debated. The topology of the magnetic field lines connected to polar cap arcs can be inferred from the in-situ observation of particles. The detection of plasma sheet-like ion and electron populations points toward a closed field line topology while the detection of polar rain-like electrons and the absence of ion precipitation points toward an open field line topology. Another means of inferring the magnetic field line topology is to investigate the conjugacy of polar cap arcs. Conjugate observation of polar cap arcs in both hemispheres fits with a closed field line topology while non-conjugate polar cap arcs rather suggest an open field line topology. The ionospheric convection within and around polar cap arcs can also provide information on the magnetic field topology.

Over the last 10 years or so, new analysis methods and data sets have suggested that polar cap arcs forming on both topologies may occur. That is, there is more than one formation mechanism of polar cap arcs. Hosokawa et al. (2011) found, in a statistical study using ground-based images, two distinct types of polar cap arcs based on their motion. They found the motion of some of the arcs to be dependent on the sign of the IMF  $B_y$  component, whilst others moved completely independently from it. They suggested that the motion of the  $B_y$ -dependent arcs is caused by flux transfer due to lobe reconnection suggesting that the plasma source for these arcs is on or adjacent to open field lines. As the  $B_y$ -independent arcs are seemingly unaffected by lobe reconnection, Hosokawa et al. (2011) argue that they are formed on closed field lines. However, Reidy et al. (2017) suggested that the motion pattern observed by Hosokawa et al. (2011) could alternatively be explained by polar cap convection as outlined by Milan et al. (2005) (a closed field line mechanism discussed in Sect. 2.2). Newell et al. (2009), based on DMSP observations of particle precipitation at low altitudes, suggested that there are three different ‘types’ of polar cap arcs, two of which occur on closed field lines and the other on open field lines. The first type discussed by Newell et al. (2009), lacks ion precipitation and thus likely occurs on open magnetic field lines, formed by accelerated polar rain (discussed in Sect. 1.3). Such arcs likely correspond to the type B polar showers as defined by Shinohara and Kokubun (1996) and to the Sun-aligned arcs discussed in Reidy et al. (2017, 2018) (see also Sect. 1.3). Such polar cap arcs



compatible with an open field line topology are associated with weak emissions. Of the two closed field line arcs (both of which are associated with plasma sheet-like ion and electron precipitation, which are consistent with the type A polar showers defined by Shinohara and Kokubun 1996), one is suggested to form on the contracted field lines of the auroral oval (and hence not actually occurring within the polar cap), and the other is completely detached from it and considered to be a more classical 'TPA' (as discussed in Sect. 1.1). However, these categorizations can be problematic when considering TPA's which form on one oval side before moving poleward and becoming 'detached' (as discussed in Sect. 1.1 and shown in Fig. 2). It is therefore necessary to look at more than one time instance to determine the nature of the arc, for example by using measurements from the multiple DMSP spacecraft.

The two possibilities (open and closed field lines) are not necessarily mutually exclusive as illustrated by the simultaneous observation of polar cap arcs on open and closed magnetic field lines by Reidy et al. (2017) (see Sect. 3.3). Due to the low altitude orbit of DMSP, the SSUSI observations could be considered to be an intermediary between ground-based and spacecraft observations. Conflicting reports suggesting polar cap arcs occur around 40% of the time in ground-based data (Valladares et al. 1994) but only 10% in UV images from high latitude spacecraft (Kullen et al. 2002) have led to some confusion. It is most likely that these differences are due to ground-based studies being able to measure weaker Sun-aligned arcs (consistent with open field lines) that are below sensitivity thresholds of UV imagers on board high-altitude spacecraft, which predominantly observe the larger-scale theta aurora (consistent with closed field lines). Reidy et al. (2018) observed polar cap arcs 20% of the time when surveying the SSUSI images over 4 months in 2015. This value is between the previous estimates discussed above and perhaps suggests that the SSUSI images could bridge the gap between the contradicting ground-based versus high altitude spacecraft observations.

In addition, some polar cap arcs do not neatly fit in the closed or open field line category. For instance, the second category of polar cap arcs discussed in Newell et al. (2009), is associated with ion and electron precipitation, about the auroral oval in particle observations, and is commonly associated with multiple convection reversals in their vicinity. These observational facts are not compatible with a closed or open magnetic field line topology. Similarly, apparently contradictory observations were reported by the Cluster satellites at higher altitude. A statistical study by Maggiolo et al. (2011) of field aligned acceleration regions above the polar caps showed that a plasma sheet-like ion population coexists with polar rain like electrons for 40% of the events. This is not consistent with a closed or an open field line topology. For the other 60% of the events, no ions could be detected, consistent with an open magnetic field line topology. However, it appears that the isotropic ion density was highly variable, from typical plasma sheet densities down to very low density without a sharp delimitation. Consequently, the distinction between events accompanied or not by plasma sheet like ions is dependent on the sensitivity of the ion detector on board Cluster. It raises questions about the impact of instrument sensitivity when using particle observations to determine the magnetic field line topology as also pointed out by Reidy et al. (2018). Furthermore, the observation of non-conjugate large-scale transpolar arcs by Østgaard et al. (2003, 2007) (discussed in Sect. 3.5) seems in contradiction with a closed or an open field line topology and remains to be explained.

### 5.3 Source of Polar Cap Arc Plasmas

In situ observations of plasma structure associated with polar cap arcs made by spacecraft at higher altitudes ( $> 8 R_E$ ) have been relatively rare until recently due to the lack of regular

coverage of the high-altitude lobe. The only pre-2000 high-altitude in situ observation we are aware of was reported by Huang et al. (1987, 1989), who showed ISEE observations (at  $22 R_E$  down-tail and  $Z_{GSM} = -8 R_E$ ) of ‘filamentary’ structures of energetic plasma in the lobes, whilst the lower-altitude Dynamics Explorer 1 satellite (apogee  $3.65 R_E$ ) observed a transpolar arc. The authors interpreted their observations as spatial filaments somehow protruding from the plasma sheet. The launch of Cluster has transformed this position, providing regular observations of the lobe in an era in which global-scale imaging of the polar cap region has been made possible by Polar, IMAGE and DMSP. Given the lifetimes of the Polar and IMAGE missions in particular, data from the period 2000–2005 is particularly rich. Nonetheless, it took a while for such data to be exploited. Shi et al. (2013) reported observations of what they termed ‘solar wind entry events’ which were similar in nature to those observed by Huang et al. (1987, 1989). A statistical analysis revealed that these ‘entry events’ occurred preferentially under northward IMF conditions; coupled with the fact that the pitch angle distribution was nearly isotropic and the proton energy was similar to that typically observed in the cusp or solar wind, Shi et al. (2013) interpreted their observations in the framework of solar wind plasma entering through the mechanism of lobe reconnection. Fear et al. (2014) presented observations of uncharacteristically hot plasma observed in the southern hemisphere magnetotail lobe; the location of the spacecraft mapped to a transpolar arc observed by IMAGE. They interpreted their observations differently from preceding studies in two respects: firstly, they interpreted the observation of multiple instances of the hot plasma as due to the back-and-forth motion of the transpolar arc in response to changing IMF  $B_y$  conditions (consistent with the IMAGE observations, and distinct from the interpretation of spatially separated filaments by Huang et al. 1987, 1989); secondly, they interpreted the hot plasma distribution as being essentially a plasma sheet population formed as a result of the magnetotail reconnection process advocated by Milan et al. (2005) (supported by the observation of a double loss cone in the plasma distribution, and contrary to the Shi et al. (2013) interpretation of direct solar wind entry).

Several subsequent studies have investigated this phenomenon further. Some have adopted the interpretation of direct solar wind entry proposed by Shi et al. (2013): Mailyan et al. (2015) reported a conjunction between plasma populations of the type observed by Shi et al. (2013) and a transpolar arc, interpreted in the framework of direct solar wind entry, implicitly placing the transpolar arc on open magnetic field lines, and Gou et al. (2016) performed a statistical analysis, arguing that observed dependencies could be explained by IMF control of the high latitude reconnection process. Others have sided with a closed field line topology formed by magnetotail reconnection: Fear et al. (2015) argued that if transpolar arcs are formed by magnetotail reconnection, then an observed interaction between a transpolar arc and the cusp spot (Frey et al. 2002) indicated that the high latitude reconnection process (indicated by the presence of the cusp spot) was actually opening the closed magnetic flux associated with the transpolar arc. More recently, Nowada et al. (2018) has provided in situ observations of the cusp region close to a transpolar arc. However, these subsequent studies have assumed one interpretation or the other—there is certainly scope for testing these two competing hypotheses further. If, as appears to be the case from multiple case studies, the appearance of hot plasma-sheet-like or solar-wind-like plasma in the lobes is associated with transpolar arcs, then the question of whether these populations are caused by direct solar wind entry or magnetotail reconnection is intrinsically linked to whether the corresponding transpolar arcs are on open or closed magnetic field lines (Sect. 5.2).

## 5.4 Connection with Substorm Triggering

The increased probability of observing polar cap arcs during periods of northward IMF leads to the presumption that polar cap arcs are associated with an inactive state of the magnetosphere. It is therefore surprising to see that polar cap arcs can in fact coexist with substorm disturbances. The two features can even be optically connected to each other. Whether this suggests a physical relation, or is merely a coincidence of independent processes, has been a subject of a long debate and still remains a puzzle. The complexity is partially due to the variable relation between the evolution sequences of polar cap arcs and substorms as reviewed below, and partially due to the lack of understanding of the magnetotail configuration with the presence of polar cap arcs.

Murphree et al. (1987, 1993, 1994) identified events where polar cap arcs are connected to the nightside auroral oval and found that the connection points are often associated with substorm-like intensifications. The connection points tend to be located at one end of the intensifications, rather than at any point along the intensifications. As the intensifications move eastward or westward, polar cap arcs move with them. Polar cap arcs can maintain their forms well into the substorm expansion phase, and then fade or rotate to join the oval. Henderson et al. (1996) found the substorm bulge does not necessarily occur on one side of polar cap arcs and can expand across the arcs. Again polar cap arcs persist well into the expansion phase and start to fade during the expansion phase.

On the other hand, Shepherd et al. (1990) and Nielsen et al. (1993) found that polar cap arcs fade or even disappear before substorm onset, and can re-brighten or reappear after the onset. The timing of the onset does not seem to have a very clear relation with the timing of arc fading. Instead, arcs fade around the start of substorm growth phase (Shepherd et al. 1990), or minutes before the onset when there is an overall dimming of the nightside auroral oval (Nielsen et al. 1993). Wu et al. (1991) found that polar cap arcs briefly intensify before fading. The intensification and/or the onset of fading occurs during the growth phase or near the start of the expansive phase of substorms. The fading stops at the beginning of the recovery phase. Spann et al. (1998) observed several polar arcs developing following a pseudo-breakup or a small substorm while the IMF  $B_z$  was strongly negative. While most of them dissipate by the time of the onset of a following substorm, one persists into the onset. Craven et al. (1986) noted a polar cap arc newly forming during a substorm, appearing first at local midnight and lengthening sunward to noon. Gusev and Troshichev (1990) also detected a polar cap arc formed at the beginning of a substorm. According to Kullen et al. (2002), TPAs typically fade some 10 s of minutes up to 1–2 hours after the onset of substorms.

A statistical examination of the time variation of polar cap arc intensity relative to substorm onset was conducted by Weygand et al. (2001). They categorized their database based on the location of polar cap arcs, dawnside or duskside. The intensity was found to vary significantly. The intensity of the duskside arcs decreased until onset, while that of the dawnside arcs showed a minimum intensity about 850 s before onset and then increased. The authors hence infer a weak interaction between polar cap arcs and substorms and suggest that the disruption of polar cap arcs is most likely due to an indirect disruption of the magnetotail convection caused during the substorm growth phase.

Recently, Nishimura et al. (2013) and Zou et al. (2015) studied the polar cap arc-substorm relation from a different perspective, where they examined the timing when polar cap arcs contact the nightside auroral oval and the onset of substorm-like intensifications (see Fig. 23). They took advantage of a network of ground-based imagers which could resolve the structures of polar cap arcs and the auroral oval in more detail than the previous spaceborne imaging, without sacrificing the spatial coverage. They found that as polar cap arcs

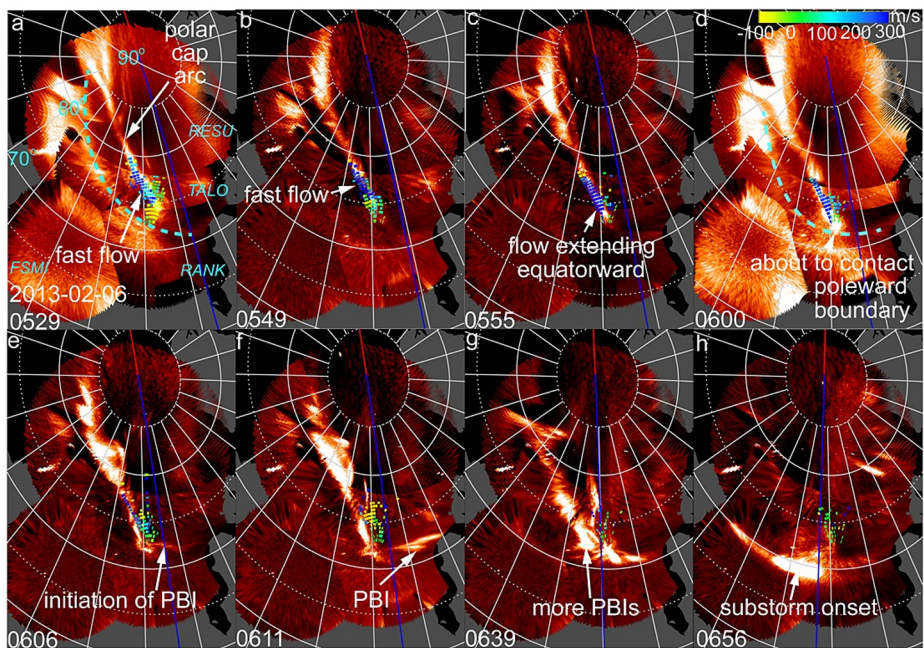


**Fig. 23** (a–h) Snapshots (630.0 nm) showing the association of a polar cap arc to PBI activity within a thick auroral oval on 6 February 2013. White lines are isocontours every  $5^\circ$  in magnetic latitude and every  $15^\circ$  longitude in Altitude Adjusted Corrected Geomagnetic Coordinates. The blue and red lines mark the midnight and noon meridian. A running median intensity over 2 h has been subtracted except for (a) and (d). (a) and (d) show absolute intensity and retain the faint and continuous emission from the nightside auroral oval, and the poleward boundary of the oval is identified and marked as the dashed light blue curve. Radar measurements (0–20 range gates) from SuperDARN at RKN station are also shown (Zou et al. 2015)

extend equatorward from high latitude, their contact with the nightside auroral poleward boundary is associated with new and substantial intensifications within the oval for 85% of the time. These intensifications statistically occur within 10 min and  $\pm 1$  h MLT from the contact. They appear as poleward boundary intensifications (PBIs) in a thick auroral oval, which can be followed by subsequent substorm activity. Or they appear as an intensification of the only resolvable arc within a thin oval, which can also exhibit substantial substorm-like poleward expansion. Since the studied polar cap arcs are associated with enhanced equatorward-directed plasma flows in the polar cap, the authors interpret the sequence as fast equatorward lobe flows compressing the plasma sheet and triggering disturbances within the plasma sheet.

## 6 Summary

Since the previous review paper by Zhu et al. (1997) we have obtained new understanding about polar cap arcs by investigating observations of various space-based and ground-based instruments. Still, however, there are several unclarified issues regarding the generation, classification and dynamics of polar cap arcs, which are summarized as follows:

- ✓ **Classification of polar cap arcs:** In this review paper, the polar cap arcs are classified into three categories, large-scale TPA, small-scale Sun-aligned arcs, and polar rain au-

rorra. In addition to these three, we introduced horse-collar aurora in possible relation to Sun-aligned arcs. However, it is still unclear if this classification is appropriate when we consider the source mechanisms of the arcs. For example, the Sun-aligned arc detected by ground-based all-sky cameras may simply be a small version of TPA seen in global imaging from satellites. Not only that, it has not yet been clarified what differentiate small-scale Sun-aligned arcs, polar rain aurora and horse-collar aurora, which could be revealed by combining ground-based observations of Sun-aligned arcs with those of polar rain aurora and Horse-collar aurora from space-based observations, for example by the DMSP SSUSI instrument. The classification of the polar cap arcs should be discussed in close association with their source mechanisms.

- ✓ **Generation mechanism:** The review paper introduces 5 different generation mechanisms of polar cap arcs, 1) IMF  $B_y$  switching and resultant twist of the magnetotail, 2) intrusion of closed flux into the polar cap by transient nightside reconnection (TRINNI), 3) interchange instability, 4) plasma sheet thickening, and 5) dayside reconnection driving processes. Most of these mechanisms have been proposed since the previous review by Zou et al. (1997), indicating that our understanding of the generation of polar cap arcs has progressed in the last two decades. From this stage, we should discuss if one of these processes can explain all the types of polar cap arcs, or polar cap arcs can be produced by multiple different processes, based on the previous observational evidence.
- ✓ **Dawn-dusk motion:** The well-known IMF  $B_y$  control of the dawn-dusk motion of polar cap arcs can be explained by the model of Milan et al. (2005) based on the flux transportation by the lobe reconnection. However, some fractions of the arcs on the dawnside are known to move poleward irrespective of the sign of IMF  $B_y$ . The mechanism of such  $B_y$ -independent arcs should be discussed to fully understand the dynamics of polar cap arcs. In addition, it should be examined how the small-scale plasma flow (i.e., localized shear flow) in the vicinity of the arcs is embedded within the large-scale convection system, for example visualized by SuperDARN, during northward IMF intervals.
- ✓ **Is the polar cap field-line open or closed?:** There is clear evidence for polar cap arcs occurring on open field lines and for polar cap arcs occurring on closed field lines which could easily be explained by different formation mechanisms. However, there exists a grey zone, with polar cap arcs for which the magnetic field line configuration cannot be determined experimentally. This remains one of the key issues associated with polar cap arcs. The knowledge of the magnetic field line topology is of prime importance to understand the formation mechanism of polar cap arcs. The main questions surrounding this issue are: If the arcs are occurring on open field lines, how are particles being accelerated to such high energies? And, if they are occurring on closed field lines, what is the configuration of the Earth's magnetotail? These questions should be addressed when we discuss the generation process of polar cap arcs.
- ✓ **Relation to the substorm triggering process:** Recent observations indicated that intensifications of the poleward boundary of the main auroral oval (PBI) occur when equatorward progressing polar cap arcs arrive at the poleward boundary and that those PBIs are followed by the substorm-like activity. However, an actual mechanism occurring in the magnetotail probably near the interface between the lobe and plasma sheet is still unclear. We should tackle this problem by combining a network of ground-based observations with in-situ satellite observations and MHD simulations having sufficient spatial resolution.

To answer all the questions summarized here, it is needed to combine all the available observations and numerical simulations. Now we are able to use several ground-based all-sky cameras in North America, Scandinavia and Antarctica, global convection measurements by

SuperDARN, localized high-resolution observations of ionospheric plasma by several incoherent scatter radars. We can also utilize space-based measurements by the DMSP, Cluster, THEMIS (Time History of Events and Macroscale Interactions) and MMS (Magnetospheric Multiscale) satellites for observing optical and particle characteristics of polar cap arcs. Combination of those observations with recently developing high spatial resolution MHD simulations will lead us to the further understanding of the nature and origin of polar cap arcs. One of the big difficulties in reaching complete understanding of the nature of polar cap arcs is the lack of continuous interhemispheric observations in the polar cap region. We suggest that the development of a twin-spacecraft mission to provide interhemispheric observations of the auroras is a high priority to advance auroral research in general, and the understanding of polar cap auroras in particular. What we really need is instruments constantly viewing the entire auroral region (i.e. global auroral imagers) with as high resolution as possible in time and space, that stay for several years above both the northern and southern polar cap.

**Acknowledgements** K.H. is supported by JSPS Kakenhi (26302006). K.H., A.K., S.M., R.M., R.F. are supported by the International Space Science Institutes (ISSI) International Team program. J.R. was supported by Natural Environment Research Council studentship NE/L002531/1, R.F. by Science and Technology Facilities Council Consolidated Grant ST/R000719/1, and S.M. by STFC Consolidated Grant ST/N000749/1. Y.Z. is supported by UCAR's Cooperative Programs for the Advancement of Earth System Science (Jack Eddy Postdoctoral Fellowship), and by National Science Foundation (AGS-1664885). H.F. was supported by NSF award AGS-1004736 and NASA's Explorers Program through contracts NNG12FA45C and NNG12FA42I.

**Publisher's Note** Springer Nature remains neutral with regard to jurisdictional claims in published maps and institutional affiliations.

**Open Access** This article is licensed under a Creative Commons Attribution 4.0 International License, which permits use, sharing, adaptation, distribution and reproduction in any medium or format, as long as you give appropriate credit to the original author(s) and the source, provide a link to the Creative Commons licence, and indicate if changes were made. The images or other third party material in this article are included in the article's Creative Commons licence, unless indicated otherwise in a credit line to the material. If material is not included in the article's Creative Commons licence and your intended use is not permitted by statutory regulation or exceeds the permitted use, you will need to obtain permission directly from the copyright holder. To view a copy of this licence, visit <http://creativecommons.org/licenses/by/4.0/>.

## References

- M. Ashrafi, ASK: Auroral structure and kinetics in action. *Astron. Geophys.* **48**(4), 4.35–4.37 (2007)
- D.N. Baker, S.J. Bame, W.C. Feldman, J.T. Gosling, R.D. Zwickl, J.A. Slavin, E.J. Smith, Strong electron bidirectional anisotropies in the distant tail-ISEE 3 observations of polar rain. *J. Geophys. Res.* **91**, 5637–5662 (1986). <https://doi.org/10.1029/JA091iA05p05637>
- F.T. Berkey, L.L. Cogger, S. Ismail, Y. Kamide, Evidence for a correlation between Sun-aligned arcs and the interplanetary magnetic field direction. *Geophys. Res. Lett.* **3**, 145–147 (1976). <https://doi.org/10.1029/GL003i003p00145>
- J. Bonnell, R.C. Elphic, S. Palfery, R.J. Strangeway, W.K. Peterson, D. Klumpar, C.W. Carlson, R.E. Ergun, J.P. McFadden, Observations of polar cap arcs on FAST. *J. Geophys. Res.* **104**, 12,669 (1999)
- W.J. Burke, M.S. Gussenhoven, M.C. Kelley, D.A. Hardy, F.J. Rich, Electric and magnetic field characteristics of discrete arcs in the polar cap. *J. Geophys. Res.* **87**(A4), 2431–2443 (1982). <https://doi.org/10.1029/JA087iA04p02431>
- H.C. Carlson, S.W.H. Cowley, Accelerated polar rain electrons as the source of Sun-aligned arcs in the polar cap during northward interplanetary magnetic field conditions. *J. Geophys. Res.* **110**, A05302 (2005). <https://doi.org/10.1029/2004JA010669>
- H.C. Carlson, R.A. Heelis, E.J. Weber, J.R. Sharber, Coherent mesoscale convection patterns during northward interplanetary magnetic field. *J. Geophys. Res.* **93**(A12), 14501–14514 (1988). <https://doi.org/10.1029/JA093iA12p14501>

- J.A. Carter, S.E. Milan, R.C. Fear, A. Kullen, M.R. Hairston, Dayside reconnection under interplanetary magnetic field  $B_y$ -dominated conditions: The formation and movement of bending arcs. *J. Geophys. Res. Space Phys.* **120**, 2967–2978 (2015). <https://doi.org/10.1002/2014JA020809>
- J.A. Carter, S.E. Milan, R.C. Fear, M.-T. Walach, Z.A. Harrison, L.J. Paxton, B. Hubert, Transpolar arcs observed simultaneously in both hemispheres. *J. Geophys. Res. Space Phys.* **122**(6), 6107–6120 (2017). <https://doi.org/10.1002/2016JA023830>
- S.-W. Chang et al., A comparison of a model for the theta aurora with observations from Polar Wind and SuperDARN. *J. Geophys. Res.* **103**, 17,367 (1998)
- G. Chisham, M. Lester, S.E. Milan, M.P. Freeman, W.A. Bristow, A. Grocott, K.A. McWilliams, J.M. Ruohoniemi, T.K. Yeoman, P.L. Dyson, R.A. Greenwald, T. Kikuchi, M. Pinnock, J.P.S. Rash, N. Sato, G.J. Sofko, J.-P. Villain, A.D.M. Walker, A decade of the Super Dual Auroral Radar Network (SuperDARN): Scientific achievements, new techniques and future directions. *Surv. Geophys.* **28**, 33–109 (2007). <https://doi.org/10.1007/s10712-007-9017-8>
- S.W.H. Cowley, Magnetospheric asymmetries associated with the y-component of the IMF. *Planet. Space Sci.* **29**, 79 (1981)
- J.D. Craven, L.A. Frank, C.T. Russell, E.J. Smith, R.P. Lepping, Global auroral responses to magnetospheric compressions by shocks in the solar wind: two case studies, in *Solar Wind–Magnetosphere Coupling*, Y. Kamide, J.A. Slavin (Terra Scientific, Tokyo, 1986), p. 367. 1986
- J.D. Craven, J.S. Murphree, L.L. Cogger, L.A. Frank, Simultaneous optical observations of transpolar arcs in the two polar caps. *Geophys. Res. Lett.* **18**, 2297–2300 (1991). <https://doi.org/10.1029/91GL02308>
- N.U. Crooker, F.J. Rich, Lobe cell convection as a summer phenomenon. *J. Geophys. Res.* **98**, 13,403–13,407 (1993)
- J.A. Cumnock, High-latitude aurora during steady northward interplanetary magnetic field and changing IMF  $B_y$ . *J. Geophys. Res.* **110**, A02304 (2005). <https://doi.org/10.1029/2004JA010867>
- J.A. Cumnock et al., Evolution of the global aurora during positive IMF  $B_z$  and varying IMF  $B_y$  conditions. *J. Geophys. Res.* **102**, 17,489–17,497 (1997). <https://doi.org/10.1029/97JA01182>
- J.A. Cumnock, J.R. Sharber, R.A. Heelis, L.G. Blomberg, G.A. Germany, J.F. Spann, W.R. Coley, Interplanetary magnetic field control of theta aurora development. *J. Geophys. Res.* (2002). <https://doi.org/10.1029/2001JA009126>
- J.A. Cumnock, L.G. Blomberg, I.I. Alexeev, E.S. Belenkaya, S.Y. Bobrovnikov, V.V. Kalegaev, Simultaneous polar aurorae and modelled convection patterns in both hemispheres. *Adv. Space Res.* **38**, 1685–1693 (2006)
- J.A. Cumnock, L.G. Blomberg, A. Kullen, T. Karlsson, K.T. Sundberg, Small-scale characteristics of extremely high latitude aurora. *Ann. Geophys.* **27**, 3335–3347 (2009). <https://doi.org/10.5194/angeo-27-3335-2009>
- H. Dahlgren, G. Perry, J.-P. St-Maurice, T. Sundberg, K. Hosokawa, J.L. Semeter, M.J. Nicolls, K. Shiokawa, 3D imaging reveals electrodynamic of polar cap aurora. *News Rev. Astron. Geophys.* **55** (2014). <https://doi.org/10.1093/astrogeo/atu215>
- H. Dahlgren, B.S. Lanchester, N. Ivchenko, D.K. Whiter, Electrodynamic and energy characteristics of aurora at high resolution by optical methods. *J. Geophys. Res. Space Phys.* **121**, 5966–5974 (2016). <https://doi.org/10.1002/2016JA022446>
- R.D. Elphinstone, K. Jankowska, J.S. Murphree, L.L. Cogger, The configuration of the auroral distribution for interplanetary magnetic field  $B_z$  northward, 1, IMF  $B_x$  and  $B_y$  dependencies as observed by the Viking satellite. *J. Geophys. Res.* **95**, 5791 (1990)
- S. Eriksson, J.B.H. Baker, S.M. Petrincec, H. Wang, F.J. Rich, M. Kuznetsova et al., On the generation of enhanced sunward convection and transpolar aurora in the high-latitude ionosphere by magnetic merging. *J. Geophys. Res.* **110**, A11218 (2005). <https://doi.org/10.1029/2005JA011149>
- G.J. Fasel, Dayside poleward moving auroral forms: A statistical study. *J. Geophys. Res.* **100**, 11,891–11,905 (1995). <https://doi.org/10.1029/95JA00854>
- R.C. Fear, The northward IMF magnetosphere, in *Magnetospheres in the Solar System*, ed. by R. Maggiolo, N. André, H. Hasegawa, D. Welling. AGU Centennial Monograph (Wiley, New York, 2019), in press
- R.C. Fear, S.E. Milan, The IMF dependence of the local time of transpolar arcs: Implications for formation mechanism. *J. Geophys. Res.* **117**, A03213 (2012a). <https://doi.org/10.1029/2011JA017209>
- R.C. Fear, S.E. Milan, Ionospheric flows relating to transpolar arc formation. *J. Geophys. Res.* **117**, A09230 (2012b). <https://doi.org/10.1029/2012JA017830>
- R.C. Fear, S.E. Milan, R. Maggiolo, A.N. Fazakerley, I. Dandouras, S.B. Mende, Direct observation of closed magnetic flux trapped in the high-latitude magnetosphere. *Science* **346**, 1506–1510 (2014). <https://doi.org/10.1126/science.1257377>
- R.C. Fear, S.E. Milan, J.A. Carter, R. Maggiolo, The interaction between transpolar arcs and cusp spots. *Geophys. Res. Lett.* **42**, 9685–9693 (2015). <https://doi.org/10.1002/2015GL066194>

- Y.I. Feldstein, P.T. Newell, I. Sandahl, J. Woch, S.V. Leontjev, V.G. Vorobjev, Structure of auroral precipitation during a theta aurora from multisatellite observations. *J. Geophys. Res.* **100**(A9), 17429–17442 (1995). <https://doi.org/10.1029/95JA00379>
- L.A. Frank, J.D. Craven, Imaging results from Dynamics Explorer 1. *Rev. Geophys.* **26**, 249 (1988)
- L.A. Frank, J.D. Craven, K.L. Ackerson, M.R. English, R.H. Eather, R.L. Carovillano, Global auroral imaging instrumentation for the Dynamics Explorer Mission. *Space Sci. Instrum.* **5**, 369–393 (1981)
- L.A. Frank, J.D. Craven, J.L. Burch, J.D. Winningham, Polar views of the Earth's aurora with dynamics explorer. *Geophys. Res. Lett.* **9**, 1001–1004 (1982). <https://doi.org/10.1029/GL009i009p01001>
- L.A. Frank, J.D. Craven, D.A. Gurnett, S.D. Shawhan, J.L. Burch, J.D. Winningham et al., The theta aurora. *J. Geophys. Res.* **91**, 3177–3224 (1986). <https://doi.org/10.1029/JA091iA03p03177>
- H.U. Frey, Localized aurora beyond the auroral oval. *Rev. Geophys.* **45**, RG1003 (2007). <https://doi.org/10.1029/2005RG000174>
- H.U. Frey, S.B. Mende, T.J. Immel, S.A. Fuselier, E.S. Claflin, J.-C. Gerard, B. Hubert, Proton aurora in the cusp. *J. Geophys. Res.* **107**, 1091 (2002). <https://doi.org/10.1029/2001JA900161>
- H.U. Frey et al., Dayside aurora. *Space Sci. Rev.* (2019, this issue). <https://doi.org/10.1007/s11214-019-0617-7>
- I.V. Golovchanskaya, A. Kullen, Y.P. Maltsev, H. Biernat, Ballooning instability at the plasma sheet-lobe interface and its implications for polar arc formation. *J. Geophys. Res.* **111**, A11216 (2006). <https://doi.org/10.1029/2005JA011092>
- X.C. Gou, Q.Q. Shi, A.M. Tian, W.J. Sun, M.W. Dunlop, S.Y. Fu, Q.G. Zong, G. Facsko, M. Nowada, Z.Y. Pu, B. Mailyan, T. Xiao, X.C. Shen, Solar wind plasma entry observed by Cluster in the high-latitude magnetospheric lobes. *J. Geophys. Res.* **121**, 4135–4144 (2016). <https://doi.org/10.1002/2015JA021578>
- A. Goudarzi, M. Lester, S.E. Milan, H.U. Frey, Multi-instrumentation observations of a transpolar arc in the northern hemisphere. *Ann. Geophys.* **26**, 201–210 (2008). <https://doi.org/10.5194/angeo-26-201-2008>
- A. Grocott, S.W.H. Cowley, J.B. Sigwarth, Ionospheric flow during extended intervals of northward but  $B_y$ -dominated IMF. *Ann. Geophys.* **21**, 509–538 (2003)
- A. Grocott, S.V. Badman, S.W.H. Cowley, T.K. Yeoman, P.J. Cripps, The influence of IMF  $B_y$  on the nature of the nightside high-latitude ionospheric flow during intervals of positive IMF  $B_z$ . *Ann. Geophys.* **22**, 1755–1764 (2004)
- M.G. Gusev, O.A. Troshichev, Hook-shaped arcs in dayside polar cap and their relationship to the IMF. *Planet. Space Sci.* **34**, 489 (1986)
- M.G. Gusev, O.A. Troshichev, Relation of sun-aligned arcs to polar cap convection and magnetic disturbances. *J. Atmos. Sol.-Terr. Phys.* **38**, 1–11 (1990)
- M.S. Gussenhoven, Extremely high latitude auroras. *J. Geophys. Res.* **87**, 2401–2412 (1982). <https://doi.org/10.1029/JA087iA04p02401>
- D.A. Hardy, Intense fluxes of low-energy electrons at geomagnetic latitudes above  $85^\circ$ . *J. Geophys. Res.* **89**, 3883–3892 (1984). <https://doi.org/10.1029/JA089iA06p03883>
- D.A. Hardy, W.J. Burke, M.S. Gussenhoven, DMSP optical and electron measurements in the vicinity of polar cap arcs. *J. Geophys. Res.* **87**, 2413–2430 (1982). <https://doi.org/10.1029/JA087iA04p02413>
- D.A. Hardy, M.S. Gussenhoven, K. Riehl, R. Burkhardt, N. Heinemann, T. Schumaker, The Characteristics of polar cap precipitation and their dependence on the interplanetary magnetic field and the solar wind, in *Solar Wind Magnetosphere Coupling, Astrophysics and Space Science Library*, vol. 126, ed. by Y. Kamide, J.A. Slavin (Reidel, Dordrecht, 1986), pp. 575–604
- M.G. Henderson, J.S. Murphree, J.M. Weygand, Observations of auroral substorms occurring together with preexisting “quiet time” auroral patterns. *J. Geophys. Res.* **101**, 24,621 (1996)
- E.W. Hones Jr., J.D. Craven, L.A. Frank, D.S. Evans, P.T. Newell, The horse-collar aurora: A frequent pattern of the aurora in quiet times. *Geophys. Res. Lett.* **16**, 37 (1989)
- K. Hosokawa, J.I. Moen, K. Shiokawa, Y. Otsuka, Motion of polar cap arcs. *J. Geophys. Res.* **116**, A01305 (2011). <https://doi.org/10.1029/2010JA015906>
- C.Y. Huang, L.A. Frank, W.K. Petersen, D.J. Williams, W. Lennartsson, D.G. Mitchell, R.C. Elphic, C.T. Russell, Filamentary structures in the magnetotail lobes. *J. Geophys. Res.* **92**, 2349–2363 (1987)
- C.Y. Huang, J.D. Craven, L.A. Frank, Simultaneous observations of a theta aurora and associated magnetotail plasmas. *J. Geophys. Res.* **94**, 10,137 (1989)
- S. Ismail, C.-I. Meng, A classification of polar cap auroral arcs. *Planet. Space Sci.* **30**, 319 (1982)
- S. Ismail, D.D. Wallis, L.L. Cogger, Characteristics of polar cap sun-aligned arcs. *J. Geophys. Res.* **82**, 4741 (1977)
- P.T. Jayachandran, K. Hosokawa, J.W. MacDougall, S. Mushini, R.B. Langley, K. Shiokawa, GPS total electron content variations associated with a polar cap arc. *J. Geophys. Res.* **114**, A12304 (2009). <https://doi.org/10.1029/2009JA014916>
- P.T. Jayachandran, K. Hosokawa, K. Shiokawa, Y. Otsuka, C. Watson, S.C. Mushini, J.W. MacDougall, P. Prıkryl, R. Chadwick, T.D. Kelly, GPS total electron content variations associated with poleward moving Sun-aligned arcs. *J. Geophys. Res.* **117**, A05310 (2012). <https://doi.org/10.1029/2011JA017423>



- P.T. Jayachandran, A. Hamza, K. Hosokawa, H. Mezaoui, K. Shiokawa, GPS amplitude and phase scintillation associated with polar cap auroral forms. *J. Atmos. Sol.-Terr. Phys.* **164**, 185–191 (2017)
- Z. Kaymaz, G.L. Siscoe, J.G. Luhmann, R.P. Lepping, C.T. Russell, Interplanetary magnetic field control of magnetotail magnetic field geometry: IMP 8 observations. *J. Geophys. Res.* **99**(A6), 11113–11126 (1994). <https://doi.org/10.1029/94JA00300>
- A. Koustov, K. Hosokawa, N. Nishitani, T. Ogawa, K. Shiokawa, Rankin Inlet PolarDARN radar observations of duskward moving Sun-aligned optical forms. *Ann. Geophys.* **26**, 2711–2723 (2008). <https://doi.org/10.5194/angeo-26-2711-2008>
- A.V. Koustov, K. Hosokawa, N. Nishitani, K. Shiokawa, H. Liu, Signatures of moving polar cap arcs in the F-region PolarDARN echoes. *Ann. Geophys.* **30**, 441–455 (2012). <https://doi.org/10.5194/angeo-30-441-2012>
- A. Kozlovsky, A. Aikio, T. Turunen, H. Nilsson, T. Sergienko, V. Safargaleev, K. Kauristie, Dynamics and electric currents of morningside Sun-aligned auroral arcs. *J. Geophys. Res.* **112**, A06306 (2007). <https://doi.org/10.1029/2006JA012244>
- A. Kullen, The connection between transpolar arcs and magnetotail rotation. *Geophys. Res. Lett.* **27**, 73–76 (2000). <https://doi.org/10.1029/1999GL010675>
- A. Kullen, Transpolar Arcs: Summary and Recent Results, in *Auroral Phenomenology and Magnetospheric Processes: Earth And Other Planets*, ed. by A. Keiling, E. Donovan, F. Bagenal, T. Karlsson (2012). <https://doi.org/10.1029/2011GM001183>
- A. Kullen, P. Janhunen, Relation of polar auroral arcs to magnetotail twisting and IMF rotation: a systematic MHD simulation study. *Ann. Geophys.* **22**, 951–970 (2004)
- A. Kullen, M. Brittner, J.A. Cumnock, L.G. Blomberg, Solar wind dependence of the occurrence and motion of polar auroral arcs: A statistical study. *J. Geophys. Res.* **107**, 1362 (2002). <https://doi.org/10.1029/2002JA009245>
- A. Kullen, J.A. Cumnock, T. Karlsson, Seasonal dependence and solar wind control of transpolar arc luminosity. *J. Geophys. Res.* **113**, A08316 (2008). <https://doi.org/10.1029/2008JA013086>
- A. Kullen, R.C. Fear, S.E. Milan, J.A. Carter, T. Karlsson, The statistical difference between bending arcs and regular polar arcs. *J. Geophys. Res. Space Phys.* **120**, 10 (2015). <https://doi.org/10.1002/2015JA021298>
- K. Lassen, On the classification of high-latitude auroras. *Geophys. Publ.* **29**, 87 (1972)
- K. Lassen, C. Danielsen, Quiet-time pattern of auroral arcs for different directions of the interplanetary magnetic field in the Y-Z plane. *J. Geophys. Res.* **83**, 5277 (1978)
- K.M. Laundal, N. Østgaard, K. Snekvik, H.U. Frey, Interhemispheric observations of emerging polar cap asymmetries. *J. Geophys. Res.* **115**, A07230 (2010). <https://doi.org/10.1029/2009JA015160>
- K.M. Laundal, J.P. Reistad, C.C. Finlay, N. Østgaard, P. Tenfjord, K. Snekvik, A. Ohma, Interplanetary magnetic field  $B_x$  component influence on horizontal and field-aligned currents in the ionosphere. *J. Geophys. Res.* **123**, 3360–3379 (2018). <https://doi.org/10.1002/2017JA024864>
- K. Liou, J.M. Ruohoniemi, P.T. Newell, R. Greenwald, C.-I. Meng, M.R. Hairston, Observations of ionospheric plasma flows within theta auroras. *J. Geophys. Res.* **110**, A03303 (2005). <https://doi.org/10.1029/2004JA010735>
- R. Maggiolo, J.A. Sauvaud, D. Fontaine, A. Teste, E. Grigorenko, A. Balogh, A. Fazakerley, G. Paschmann, D. Delcourt, H. Rème, A multi-satellite study of accelerated ionospheric ion beams above the polar cap. *Ann. Geophys.* **24**(6), 1665–1684 (2006). <https://doi.org/10.5194/angeo-24-1665-2006>
- R. Maggiolo, M. Echim, J. de Keyser, D. Fontaine, C. Jacquey, I. Dandouras, Polar cap ion beams during periods of northward IMF: Cluster statistical results. *Ann. Geophys.* **29**, 771–787. <https://doi.org/10.5194/angeo-29-771-2011> (2011)
- R. Maggiolo, M. Echim, C. Simon Wedlund, Y. Zhang, D. Fontaine, G. Lointier, J.-G. Trotignon, Polar cap arcs from the magnetosphere to the ionosphere: kinetic modelling and observations by Cluster and TIMED. *Ann. Geophys.* **30**, 283–302 (2012). <https://doi.org/10.5194/angeo-30-283-2012>
- B. Mailyan, Q.Q. Shi, A. Kullen, R. Maggiolo, Y. Zhang, R.C. Fear, Q.-G. Zong, S.Y. Fu, X.C. Gou, X. Cao, Z.H. Yao, W.J. Sun, Y. Wei, Z.Y. Pu, Transpolar arc observation after solar wind entry into the high-latitude magnetosphere. *J. Geophys. Res.* **120**, 3525–3534 (2015). <https://doi.org/10.1002/2014JA020912>
- K. Makita, C.I. Meng, S.I. Akasofu, Transpolar auroras, their particle precipitation, and IMF  $B_y$  component. *J. Geophys. Res.* **96**, 14,085 (1991)
- D. Mawson, Auroral observations at the Cape Royds station, Antarctica. *Trans. R. Soc. S. Aust.* **XL**, 151–212 (1916)
- D. Mawson, Records of the Aurora Polaris. *Australasian expedition 1911–1914. Sci. Rep. B* **11**, 5758367 (1925)
- N.C. Maynard et al., Response of the open–closed field line boundary in the evening sector to IMF changes: A source mechanism for Sun-aligned arcs. *J. Geophys. Res.* **108**(A1), 1006 (2003). <https://doi.org/10.1029/2001JA000174>

- N.C. Maynard, C.J. Farrugia, W.J. Burke, D.M. Ober, F.S. Mozer, H. Rème, M. Dunlop, K.D. Siebert, Cluster observations of the dusk flank magnetopause near the sash: Ion dynamics and flow-through reconnection. *J. Geophys. Res.* **117**, A10201 (2012). <https://doi.org/10.1029/2012JA017703>
- D.J. McEwen, Y. Zhang, A continuous view of the dawn-dusk polar cap. *Geophys. Res. Lett.* **27**, 477 (2000)
- S.B. Mende, H. Heeterdicks, H.U. Frey, M. Lampton, S.P. Geller, S. Habraken, E. Renotte, C. Jamar, P. Rochus, J. Spann, S.A. Fuselier, J.-C. Gerard, R. Gladstone, S. Murphree, L. Cogger, Far ultraviolet imaging from the IMAGE spacecraft: 1. System design. *Space Sci. Rev.* **91**, 243–270 (2000). <https://doi.org/10.1023/A:1005271728567>
- C.-I. Meng, Polar cap arcs and the plasma sheet. *Geophys. Res. Lett.* **8**, 273 (1981)
- C.-I. Meng, H.W. Kroehl, Intense uniform precipitation of low-energy electrons over the polar cap. *J. Geophys. Res.* **82**, 2305–2313 (1977). <https://doi.org/10.1029/JA082i016p02305>
- S.E. Milan, M. Lester, S.W.H. Cowley, M. Brittner, The convection and auroral response to a southward turning of the IMF: Polar UVI, CUTLASS, and IMAGE signatures of transient magnetic flux transfer at the magnetopause. *J. Geophys. Res.* **105**, 15741–15756 (2000)
- S.E. Milan, B. Hubert, A. Grocott, Formation and motion of a transpolar arc in response to dayside and nightside reconnection. *J. Geophys. Res.* **110**, A01212 (2005). <https://doi.org/10.1029/2004JA010835>
- P.F. Mizera, D.J. Gorney, D.S. Evans, On the conjugacy of the aurora: High and low latitudes. *Geophys. Res. Lett.* **14**(3), 190–193 (1987). <https://doi.org/10.1029/GL014i003p00190>
- J.S. Murphree, L.L. Cogger, Observed connections between apparent polar cap features and the instantaneous diffuse auroral oval. *Planet. Space Sci.* **29**, 1143 (1981)
- J.S. Murphree, C.D. Anger, L.L. Cogger, The instantaneous relationship between polar cap and oval auroras at times of northward interplanetary magnetic field. *Can. J. Phys.* **60**, 349 (1982)
- J.S. Murphree, L.L. Cogger, C.D. Anger, D.D. Wallis, G.G. Shepherd, Oval intensifications associated with polar arcs. *Geophys. Res. Lett.* **14**, 403–406 (1987)
- J.S. Murphree, R.D. Elphinstone, M.G. Henderson, L.L. Cogger, D.J. Hearn, Interpretation of optical substorm onset observations. *J. Atmos. Sol.-Terr. Phys.* **55**(8), 1159–1170 (1993). [https://doi.org/10.1016/0021-9169\(93\)90044-Y](https://doi.org/10.1016/0021-9169(93)90044-Y)
- J.S. Murphree, J.B. Austin, D.J. Hearn, L.L. Cogger, R.D. Elphinstone, J. Woch, Satellite observations of polar arcs. *J. Atmos. Sol.-Terr. Phys.* **56**(2), 265 (1994)
- S.M. Naehr, F.R. Toffoletto, Quantitative modeling of the magnetic field configuration associated with the theta aurora. *J. Geophys. Res.* **109**, A07202 (2004). <https://doi.org/10.1029/2003JA010191>
- P.T. Newell, C.-I. Meng, Creation of theta-auroras: the isolation of plasma sheet fragments in the polar cap. *Science* **270**, 1338 (1995)
- P.T. Newell, D. Xu, C.-I. Meng, M.G. Kivelson, Dynamical polar cap: a unifying approach. *J. Geophys. Res.* **102**, 127 (1997). 1997
- P.T. Newell, K. Liou, C.-I. Meng, M.J. Brittner, G. Parks, Dynamics of double-theta aurora: Polar UVI study of January 10–11. *J. Geophys. Res. Space Phys.* **104**(A1), 95–104 (1999). 1997
- P.T. Newell, K. Liou, G.R. Wilson, Polar cap particle precipitation and aurora: Review and commentary. *J. Atmos. Sol.-Terr. Phys.* **71**, 199–215 (2009). <https://doi.org/10.1016/j.jastp.2008.11.004>
- E. Nielsen, J.D. Craven, L.A. Frank, R.A. Heelis, Ionospheric flows associated with a transpolar arc. *J. Geophys. Res.* **95**(A12), 21,169–21,178 (1990). <https://doi.org/10.1029/JA095iA12p21169>
- E. Nielsen, R. Elphinstone, D. Hearn, J.S. Murphree, T. Potemra, Oval intensification event observed by STARE and Viking. *J. Geophys. Res.* **98**, 6163 (1993)
- Y. Nishimura, L.R. Lyons, K. Shiokawa, V. Angelopoulos, E.F. Donovan, S.B. Mende, Substorm onset and expansion phase intensification precursors seen in polar cap patches and arcs. *J. Geophys. Res.* **118**, 2034–2042 (2013). <https://doi.org/10.1002/jgra.50279>
- M. Nowada, R.C. Fear, A. Grocott, Q.-Q. Shi, Q.-G. Zong, Y. Wei, S.-Y. Fu, Z.-Y. Pu, B. Mailyan, H. Zhang, Subside of Ionospheric Flows Triggered by Magnetotail Magnetic Reconnection During Transpolar Arc Brightening. *J. Geophys. Res.* **123**, 3398–3420 (2018). <https://doi.org/10.1029/2017JA024701>
- T. Obara, M. Kitayama, T. Mukai, N. Kaya, L. Cogger, S. Murphree, Simultaneous observations of Sun-aligned polar cap arcs in both hemispheres by EXOS-C and Viking. *Geophys. Res. Lett.* **15**(7), 713–716 (1988). <https://doi.org/10.1029/GL015i007p00713>
- N. Østgaard, S.B. Mende, H.U. Frey, L.A. Frank, J.B. Sigwarth, Observations of non-conjugate theta aurora. *Geophys. Res. Lett.* **30**, 2125 (2003). <https://doi.org/10.1029/2003GL017914>
- N. Østgaard, S.B. Mende, H.U. Frey, J.B. Sigwarth, Simultaneous imaging of the reconnection spot in the opposite hemispheres during northward IMF. *Geophys. Res. Lett.* **32**, L21104 (2005). <https://doi.org/10.1029/2005GL024491>
- N. Østgaard, S.B. Mende, H.U. Frey, J.B. Sigwarth, A. Åsnes, J.M. Weygand, Auroral conjugacy studies based on global imaging. *J. Atmos. Sol.-Terr. Phys.* **69**(3), 249–255 (2007). <https://doi.org/10.1016/j.jastp.2006.05.026>

- C.J. Owen, J.A. Slavin, I.G. Richardson, N. Murphy, R.J. Hynds, Average motion, structure and orientation of the distant magnetotail determined from remote sensing of the edge of the plasma sheet boundary layer with  $E > 35$  keV ions. *J. Geophys. Res.* **100**, 185 (1995)
- L.J. Paxton, D. Morrison, Y. Zhang, H. Kil, B. Wolven, B.S. Ogorzalek et al., Validation of Remote Sensing Products Produced by the Special Sensor Ultraviolet Scanning Imager (SSUSI): A far UV Imaging Spectrograph on DMSP F16, in *Optical spectroscopic techniques, remote sensing, and instrumentation for atmospheric and space research IV*, ed. by A.M. Larar, M.G. Mlynczak. Proc. SPIE, vol. 4485 (SPIE, San Diego, 2002), pp. 338–348. <https://doi.org/10.1117/12.454268>
- G.W. Perry, H. Dahlgren, M.J. Nicolls, M. Zettergren, J.-P. St.-Maurice, J.L. Semeter, T. Sundberg, K. Hosokawa, K. Shiokawa, S. Chen, Spatiotemporally resolved electrodynamic properties of a Sun-aligned arc over Resolute Bay. *J. Geophys. Res.* **120**, 9977–9987 (2015). <https://doi.org/10.1002/2015JA021790>
- W.K. Peterson, E.G. Shelley, Origin of the plasma in a cross-polar cap auroral feature (theta aurora). *J. Geophys. Res.* **89**, 6729 (1984)
- R.L. Rairden, S.B. Mende, Properties of 6300-Å auroral emissions at South Pol. *J. Geophys. Res.* **94**(A2), 1402–1416 (1989). <https://doi.org/10.1029/JA094iA02p01402>
- J.A. Reidy, R.C. Fear, D.K. Whiter, B.S. Lanchester, A.J. Kavanagh, L.J. Paxton et al., Multi-instrument observation of simultaneous polar cap auroras on open and closed magnetic field lines. *J. Geophys. Res. Space Phys.* **122**, 4367–4386 (2017). <https://doi.org/10.1002/2016JA023718>
- J. Reidy, R.C. Fear, D. Whiter, B.S. Lanchester, A.J. Kavanagh, S.E. Milan et al., Interhemispheric survey of polar cap aurora. *J. Geophys. Res. Space Phys.* **123**, 7283–7306 (2018). <https://doi.org/10.1029/2017JA025153>
- B.V. Rezhenov, A possible mechanism for theta aurora formation. *Ann. Geophys.* **13**, 698 (1995)
- R.M. Robinson, R.R. Vondrak, K. Miller, T. Dabbs, D. Hardy, On calculating ionospheric conductances from the flux and energy of precipitating electrons. *J. Geophys. Res.* **92**(A3), 2565–2569 (1987). <https://doi.org/10.1029/JA092iA03p02565>
- J.M. Ruohoniemi, R.A. Greenwald, Statistical patterns of high-latitude convection obtained from Goose Bay HF radar observations. *J. Geophys. Res.* **101**, 9494–9510 (1996). <https://doi.org/10.1029/96JA0158>
- M. Samara, R.G. Michell, Optical and radar observations of small-scale polar cap auroral structures. *J. Atmos. Sol.-Terr. Phys.* **105–106**, 308–312 (2013)
- G.G. Shepherd, A. Steen, J.S. Murphree, Auroral boundary dynamics observed simultaneously from the Viking spacecraft and from the ground. *J. Geophys. Res.* **95**, 5845 (1990)
- Q.Q. Shi, Q.-G. Zong, S.Y. Fu, M.W. Dunlop, Z.Y. Pu, G.K. Parks, Y. Wei, W.H. Li, H. Zhang, M. Nowada, Y.B. Wang, W.J. Sun, T. Xiao, H. Reme, C. Carr, A.N. Fazakerley, E. Lucek, Solar wind entry into the high-latitude terrestrial magnetosphere during geomagnetically quiet times. *Nat. Commun.* **4**, 1466 (2013). <https://doi.org/10.1038/ncomms2476>
- I. Shinohara, S. Kokubun, Statistical properties of particle precipitation in the polar cap during intervals of northward interplanetary magnetic field. *J. Geophys. Res.* **101**, 69–82 (1996). <https://doi.org/10.1029/95JA01848>
- K. Shiokawa, K. Yumoto, K. Hayashi, T. Oguti, D.J. McEwen, A statistical study of the motions of auroral arcs in the high-latitude morning sector. *J. Geophys. Res.* **100**, 21,979–21,985 (1995). <https://doi.org/10.1029/95JA01564>
- K. Shiokawa, K. Yumoto, N. Nishitani, K. Hayashi, T. Oguti, D.J. McEwen, Y. Kiyama, F.J. Rich, T. Mukai, Quasi-periodic poleward motions of Sun-aligned auroral arcs in the high-latitude morning sector: A case study. *J. Geophys. Res.* **101**, 19,789–19,800 (1996). <https://doi.org/10.1029/96JA01202>
- K. Shiokawa, T. Ogino, K. Hayashi, D.J. McEwen, Quasi-periodic poleward motions of morningside Sun-aligned arcs: A multi-event study. *J. Geophys. Res.* **102**, 24,325–24,332 (1997). <https://doi.org/10.1029/97JA02383>
- J.-H. Shue, P.T. Newell, K. Liou, C.-I. Meng, The quantitative relationship between auroral brightness and solar EUV Pedersen conductance. *J. Geophys. Res.* **106**, 5883 (2001)
- S.P. Slinker, J.A. Fedder, D.J. McEwen, Y. Zhang, J.G. Lyon, Polar cap study during northward interplanetary magnetic field on 19 January 1998. *Phys. Plasmas* **8**, 1119 (2001)
- J.F. Spann, M. Brittnacher, R. Elsen, G.A. Germany, G.K. Parks, Initial response and complex polar cap structures of the aurora in response to the January 10, 1997 magnetic cloud. *Geophys. Res. Lett.* **25**, 2577 (1998)
- T.J. Stubbs, R.R. Vondrak, N. Østgaard, J.B. Sigwarth, L.A. Frank, Simultaneous observations of the auroral ovals in both hemispheres under varying conditions. *Geophys. Res. Lett.* **32**, L03103 (2005). <https://doi.org/10.1029/2004GL021199>
- T. Tanaka, T. Obara, M. Kunitake, Formation of the theta aurora by a transient convection during northward interplanetary magnetic field. *J. Geophys. Res.* **109**, A09201 (2004). <https://doi.org/10.1029/2003JA010271>

- T. Tanaka, T. Obara, M. Watanabe, S. Fujita, Y. Ebihara, R. Kataoka, Formation of the Sun-aligned arc region and the void (polar slot) under the null-separator structure. *J. Geophys. Res.* **122**, 4102–4116 (2017). <https://doi.org/10.1002/2016JA023584>
- T. Tanaka, T. Obara, M. Watanabe, S. Fujita, Y. Ebihara, R. Kataoka, M. Den, Cooperatives Roles of Dynamics and Topology in Generating the Magnetosphere-Ionosphere Disturbances: Case of the Theta Aurora. *J. Geophys. Res. Space Phys.* **123**(12), 9991–10008 (2018)
- A. Teste, D. Fontaine, J.-A. Sauvaud, R. Maggiolo, P. Canu, A. Fazakerley, CLUSTER observations of electron outflowing beams carrying downward currents above the polar cap by northward IMF. *Ann. Geophys.* **25**, 953–969 (2007). <https://doi.org/10.5194/angeo-25-953-2007>
- M.R. Torr, D.G. Torr, M. Zukic, R.B. Johnson, J. Ajello, P. Banks, K. Clark, K. Cole, C. Keffer, G. Parks, B. Tsurutani, J. Spann, A far ultraviolet imager for the International Solar-Terrestrial Physics mission. *Space Sci. Rev.* **71**(1–4), 329–383 (1995)
- N.A. Tsyganenko, A magnetospheric magnetic field model with a warped tail current sheet. *Planet. Space Sci.* **37**, 5 (1989)
- N.A. Tsyganenko, D.H. Fairfield, Global shape of the magnetotail current sheet as derived from Geotail and Polar data. *J. Geophys. Res.* **109**, A03218 (2004). <https://doi.org/10.1029/2003JA010062>
- C.E. Valladares, H.C. Carlson Jr., The electrodynamic, thermal, and energetic character of intense Sun-aligned arcs in the polar cap. *J. Geophys. Res.* **96**(A2), 1379–1400 (1991). <https://doi.org/10.1029/90JA01765>
- C.E. Valladares, H.C. Carlson Jr., K. Fukui, Interplanetary magnetic field dependency of stable Sun-aligned polar cap arcs. *J. Geophys. Res.* **99**, 6247–6272 (1994). <https://doi.org/10.1029/93JA03255>
- C. van der Meer, K. Oksavik, D.A. Lorentzen, L.J. Paxton, L.B.N. Clausen, Scintillation and irregularities from the nightside part of a Sun-aligned polar cap arc. *J. Geophys. Res.* **121**, 5723–5736 (2016). <https://doi.org/10.1002/2016JA022708>
- R.J. Walker, R.L. Richard, T. Ogino, M. Ashour-Abdalla, The response of the magnetotail to changes in the IMF orientation: The magnetotail's long memory. *Phys. Chem. Earth Part C* **24**, 221 (1999)
- M. Watanabe, M.R. Hairston, Observation of a unipolar field-aligned current system associated with IMF  $B_y$ -triggered theta auroras. *J. Geophys. Res.* **121**, 4483–4497 (2016). <https://doi.org/10.1002/2015JA022016>
- E.J. Weber, J. Buchau, Polar cap F-layer auroras. *Geophys. Res. Lett.* **8**(1), 125–128 (1981). <https://doi.org/10.1029/GL008i001p00125>
- J.M. Weygand, J.S. Murphree, M.G. Henderson, G.A. Enno, Simultaneous closed magnetic field line polar arcs and substorms. *J. Atmos. Terr. Phys.* **63**, 643–655 (2001). [https://doi.org/10.1016/S1364-6826\(00\)00184-X](https://doi.org/10.1016/S1364-6826(00)00184-X)
- M. Wiltberger, R.S. Weigel, W. Lotko, J.A. Fedder, Modeling seasonal variations of auroral particle precipitation in a global-scale magnetosphere-ionosphere simulation. *J. Geophys. Res.* **114**, A01204 (2009). <https://doi.org/10.1029/2008JA013108>
- J.D. Winningham, W.J. Heikkila, Polar cap auroral electron fluxes observed with Isis 1. *J. Geophys. Res.* **79**(7), 949–957 (1974). <https://doi.org/10.1029/JA079i007p00949>
- Q. Wu, T.J. Rosenberg, F.T. Berkeley, R.H. Eather, Intensification and fading of auroral arcs in the dusk-midnight sector of the polar cap. *J. Geophys. Res.* **96**(A5), 7709–7719 (1991). <https://doi.org/10.1029/91JA00256>
- J. Xing, Q. Zhang, D. Han, Y. Zhang, N. Sato, S. Zhang et al., Conjugate observations of the evolution of polar cap arcs in both hemispheres. *J. Geophys. Res. Space Phys.* **123**, 1794–1805 (2018). <https://doi.org/10.1002/2017JA024272>
- T. Yamamoto, M. Ozaki, A numerical model of the dayside aurora. *J. Geophys. Res.* **110**, A05215 (2005). <https://doi.org/10.1029/2004JA010786>
- D.Y. Yeager, L.A. Frank, Low-energy electron intensities at large distances over the Earth's polar cap. *J. Geophys. Res.* **81**, 3966–3976 (1976). <https://doi.org/10.1029/JA081i022p03966>
- Y. Zhang, D.J. McEwen, N. Kong, J.J. Sojka, L. Zhu, Horizontal electrojet associated with the sun-aligned arcs. *J. Atmos. Sol.-Terr. Phys.* **61**, 1249–1257 (1999)
- Y. Zhang, L.J. Paxton, P.T. Newell, C.I. Meng, Does the polar cap disappear under an extended strong northward IMF? *J. Atmos. Sol.-Terr. Phys.* **71**(17–18), 2006–2012 (2009)
- Y. Zhang, L.J. Paxton, Q.-H. Zhang, Z. Xing, Polar cap arcs: sun-aligned or cusp-aligned? *J. Atmos. Sol.-Terr. Phys.* **146**, 123–128 (2016)
- L. Zhu, C.E. Valladares, J.J. Sojka, R.W. Schunk, D.J. Crain, Model-observation comparison study of multiple polar cap arcs. *J. Geophys. Res.* **101**(A1), 323–333 (1996). <https://doi.org/10.1029/95JA02758>
- L. Zhu, R.W. Schunk, J.J. Sojka, Polar cap arcs: A review. *J. Atmos. Sol.-Terr. Phys.* **59**, 1087–1126 (1997). [https://doi.org/10.1016/S1364-6826\(96\)00113-7](https://doi.org/10.1016/S1364-6826(96)00113-7)
- Y. Zou, Y. Nishimura, L.R. Lyons, E.F. Donovan, K. Shiokawa, J.M. Ruohoniemi, K.A. McWilliams, N. Nishitani, Polar cap precursor of nightside auroral oval intensifications using polar cap arcs. *J. Geophys. Res.* **120**, 10,698–10,711 (2015). <https://doi.org/10.1002/2015JA021816>